Polar Biology
https://doi.org/10.1007/s00300-020-02722-2

ORIGINAL PAPER

Variability in primary productivity and bio-optical properties in the Indian sector of the Southern Ocean during an austral summer

Anvita U. Kerkar[1,5] · S. C. Tripathy[1] · P. Minu[2] · N. Baranval[3] · P. Sabu[1] · S. Patra[4] · R. K. Mishra[1] · A. Sarkar[1,6]

Received: 5 December 2019 / Revised: 30 June 2020 / Accepted: 3 August 2020

Abstract

The Southern Ocean (SO), in spite of its major contribution to global primary productivity (PP), remains underexplored in this aspect. Light being the most limiting parameter affecting primary production, it is crucial to study the ambient light field to understand PP and associated processes. The current study makes a dual effort to present PP estimates as well as understand the bio-optical variability in the Indian sector of the Southern Ocean (ISSO). Results suggest that PP was highest at Sub-Tropical Front (STF) and lowest at Polar Front-2 (PF2). Most PP profiles were characterized by subsurface maxima, indicating probable photoinhibition or micronutrient limitation at surface layer. Strong correlation between measured and satellite-based integrated PP ($R^2 = 0.94$, $RMSE = 77.48$, $p < 0.01$) indicated the efficacy of global models in their original formulation in bio-optically complex SO waters. The maximum photochemical efficiency of phytoplankton (F_v/F_m) measured by fast repetition rate fluorometry varied from 0.1–0.4, implying reduced phytoplankton photosynthetic efficiency in ISSO. The ratio between remote sensing reflectance (R_{rs})-derived phytoplankton absorption (a_{ph}) at blue-red band (B/R ratio) indicated dominance of smaller phytoplankton in surface and larger phytoplankton at subsurface. Higher Chl-a specific phytoplankton absorption (a^*_{ph}) than phytoplankton absorption (a_{ph}) suggested an adaptation of dominant phytoplankton species to low light, yet a better light harvest efficiency. However, low contribution of a_{ph} suggested a strong influence of non-phytoplankton materials to the total absorption budget. We therefore infer that, the surrounding physical environment in terms of nutrients and bio-optical variability modulated phytoplankton size class and thereby productivity more critically in the surface than in the deeper layers of ISSO.

Keywords Light absorption · Package effect · Photosynthetic parameters · Phytoplankton productivity · Southern ocean

Introduction

The Southern Ocean (SO) plays a central role in influencing the global climate change scenario owing the uniqueness of its frontal systems, the Antarctic Circumpolar Current (ACC) (Orsi et al. 1995), absence of meridional boundary and the inter-oceanic connections established between the Atlantic, Pacific and Indian Oceans (Olbers et al. 2004). In spite of its high-nutrient low-chlorophyll (HNLC) status (Trull et al. 2001; Boyd et al. 2002), the SO contributes to almost 40% of the oceanic phytoplankton primary production (PP) and acts as a carbon sink (Arrigo et al. 2008). Of late, the physicochemical and biological characteristics of the SO have been showing clear responses to climate change (Graham 2014). Hence, an improved understanding of the key biogeochemical processes like PP with respect to the ambient physical forcings is a prerequisite to address the response of the SO in Earth's climatic variability.

✉ S. C. Tripathy
sarat@ncpor.res.in

1 National Centre for Polar and Ocean Research (NCPOR), Ministry of Earth Sciences, Headland Sada, Vasco-da-Gama, Goa 403804, India

2 Central Institute of Fisheries Technology, ICAR, Willingdon Island, Kochi 682029, India

3 National Remote Sensing Centre, ISRO, Balanagar, Hyderabad 500037, India

4 National Centre for Coastal Research, Ministry of Earth Sciences, NIOT Campus, Pallikaranai, Chennai 600100, India

5 School of Earth, Ocean and Atmospheric Sciences, Goa University, Taleigao Plateau, Goa 403206, India

6 Environment and Life Sciences Research Centre, Kuwait Institute for Scientific Research Centre, Al-Jaheth Street, 13109 Shuwaikh, Kuwait

Published online: 13 August 2020

Oceanic PP plays a major role in global carbon cycle by drawing down atmospheric CO_2 to the ocean interior through the 'biological pump' (Sarmiento et al. 1998; Le Quere et al. 2007) and is strongly influenced by availability of light and supply of nutrients (macro and micro). The low primary production, regardless of the usual high-nutrient concentrations in the most parts of the SO, is attributed to three basic variables: chlorophyll-a (Chl-a), photosynthetically active radiation (PAR), and phytoplankton light absorption capacity (Behrenfeld and Falkowski 1997a). It is reported that the SO ecosystem is highly sensitive to physical forcings that influence fluctuations in light, nutrients, mixed layer depth (MLD), deep chlorophyll maximum (DCM), sea ice, upwelling, etc. (Rintoul et al. 2014), which are well-known modulators of PP in the study region. Thus, it is imperative to have a clear understanding of these factors to know the spatiotemporal variability of PP in the SO. The carbon-fixing potential of primary producers (phytoplankton) can be used as an effective tool to study biogeochemical fluxes, carbon and nutrient cycling. The dynamics in temperature, MLD, wind strength, salinity, extent and duration of sea ice are well-known modulators of the phytoplankton composition, abundance and productivity in the SO (Moline et al. 2004). In addition to these physical parameters, ocean colour studies which involve use of the spectral absorption coefficients of the dissolved and suspended particles throughout the water column are extremely important to estimate PP using remote platforms (Behrenfeld et al. 2006).

Despite its well-known global significance, a large expanse of SO still remains poorly explored due to its extremely harsh conditions and remote location. Though PP and factors controlling it in different sectors of SO have been illustrated by several studies, the reports from the Indian sector of the SO (ISSO) are scant (Tripathy et al. 2017). Some of the previous studies in the ISSO have reported productivity potential of different frontal regions using satellite-derived parameters (Jasmine et al. 2009), prevalence of regenerated PP at all the fronts except STF, seasonal and spatial variations in new PP (*f* ratios) (Mengesha et al. 1998; Thomalla et al. 2011; Gandhi et al. 2012; Prakash et al. 2015; Tripathy et al. 2018), role of DCM in PP variability (Gomi et al. 2010; Tripathy et al. 2015), influence of phytoplankton pigment package effect on PP (Tripathy et al. 2014), phytoplankton photochemical efficiency by Fast Repetition Rate fluorometry (FRRf) (Westwood et al. 2011) and effect of Island mass effect on PP variability (Blain et al. 2001).

Light is the most important determinant of PP and is attenuated in the water column by the different suspended and dissolved bio-optical constituents. Spectral Absorption coefficients of these constituents help in understanding the underwater light variability and its availability for C-fixation (Sathyendranath and Platt 2007). These in situ bio-optical measurements are extremely useful for validation of ocean colour observation from satellite sensors, predicting the amount of light used for photosynthesis (Bricaud et al. 2004) and spatiotemporal variations in phytoplankton absorption coefficients in global oceans (Lohrenz et al. 2003; Babin et al. 2003). The optical properties of SO are expected to be complex due to the dynamic hydrographic conditions (e.g. freshwater intrusion, upwelling and mixing). Studies in the SO and elsewhere have shown that freshwater intrusion could significantly change the light absorption efficiency among phytoplankton, detritus, and coloured dissolved organic matter (Babin et al. 2003; Wang et al. 2014; Tripathy et al. 2014), thus modulating the underwater light available for PP.

Though several studies have been carried out in the ISSO to explain variability of PP, rarely any (Hirawake et al. 2011) of them has explained the link between bio-optical properties and PP. Taking into account this lack of bio-optical observations in ISSO, we attempt to study the variability in ^{14}C-based PP and bio-optical properties in relation to ambient environmental parameters at different frontal zones of the ISSO. Moreover, we aim to (1) identify the dominant factors for PP variability and compare the in situ PP with the vertically generalized production model (VGPM) output, (2) use bio-optical technique like FRRf to explain the fluctuations in phytoplankton physiological parameters with respect to ambient physicochemical parameters, and (3) obtain an overall picture of light absorption budget in the study region and find its inter-linkages with photo-physiological properties (such as pigment packaging effect, photoinhibition, absorption efficiency) and PP. The present study would not only generate baseline bio-optical datasets but also would contribute towards bio-optical oceanography in relation to phytoplankton productivity in this under sampled region.

Materials and methods

Study area, sampling and hydrography

Study area (Fig. 1) comprises PF (Polar Front), SAF (Sub-Antarctic Front) and the STF (Sub-Tropical Front). In the ISSO, the PF is divided into two branches between 49° S and 52° S (PF1) and 53° S and 55° S (PF2). The branches show distinct, characteristic sea surface temperatures (SST); 4–5 °C at the Northern branch (PF1) and 2–3 °C at the southern branch (PF2) (Sokolov and Rintoul 2002). The PF also possesses unique physicochemical (Trull et al. 2001) and biological characteristics (Pavithran et al. 2012) at its two different branches and has significant contribution to biological production and biogeochemical cycling (Kemp et al. 2010). The SAF is recognized as the Northern boundary of the PF (Kostianoy et al. 2004). It bears

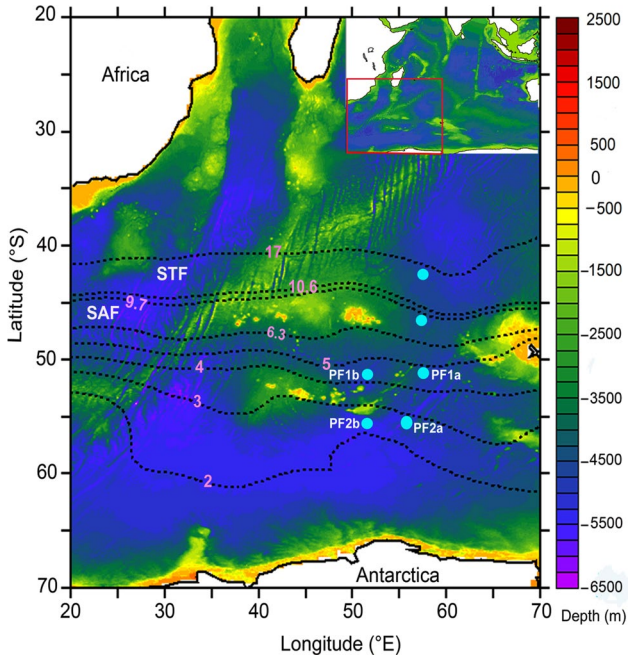

Fig. 1 Study area map showing station locations (closed circles) at STF, SAF, PF1 and PF2 in the Indian sector of Southern Ocean. Background colours indicate the bathymetry (ETOPO data). The dotted lines are sea surface temperature contours indicative of different frontal boundaries. The inset figure shows a larger perspective of the study area

an isotherm of SST at 8.1 °C and possesses a bimodal path (Moore et al. 1999). The STF is known as the most dynamic front of the SO and acts as a boundary between the saline, warm sub-tropical waters and fresh, cool sub-Antarctic waters with isohalines of 35.0 psu (Belkin and Gordon 1996). The salinity and temperature ranges from 34.6–35.0 psu and 10 and 12 °C at 100 m depth, respectively (Orsi et al. 1995).

The 8th Indian Expedition to the SO (2015) included sampling at six stations at different frontal regions. Sampling was carried out onboard ORV-*Sagar Nidhi* along the 57.5° E meridian transect (regular track of the Indian Expedition to the SO) in the ISSO during austral summer including each of the front (i.e. STF, SAF, PF1 and PF2). Water samples were collected from surface and discrete sampling depths by Niskin bottle of 10L capacity mounted on a Conductivity-Temperature-Depth (CTD, SBE 911+, USA) carousel (General Oceanics Inc., USA) and sub-sampled for further analyses. The vertical profiles of temperature, salinity, dissolved oxygen (DO), photosynthetically active radiation (PAR) were obtained from the CTD carousel. The CTD profiles were used to estimate the Brunt–Vaisala frequency (*N*), a measure of stability of the water column (Pond and Pickard 1978), using the expression,

$$N = \sqrt{-\frac{g}{\rho_0} \cdot \frac{\partial \rho}{\partial z}}$$

where g is the acceleration due to gravity, ρ_0 is the reference seawater density (1025 kg m^{-3}) and $\frac{\partial \rho}{\partial z}$ is the vertical potential density gradient. Positive, zero and negative N values indicate stable, neutral and unstable water column, respectively.

Macronutrients, chlorophyll-a and PAR

100 ml of water samples were collected onboard for the analysis of nitrate (NO_3), phosphate (PO_4) and silicate (SiO_4). These water samples were stored at − 40 °C until further analysis. The water samples were analysed in the NCPOR laboratory for the concentration of respective nutrients using a segmented flow analyzer (SKALAR) following the standard methodology for seawater analysis (UNESCO 1994). The precision of detection (limits) for NO_3, PO_4 and SiO_4were ± 0.06 (± 0.07), ± 0.003 (± 0.004), and ± 0.06 (± 0.04) µM, respectively. The water samples filtered on 47 mm Whatman GF/F filters were extracted in 90% acetone in cold, dark conditions overnight and analysed fluorometrically (10-AU, Turner Designs with a detection limit of 0.02 mg m^{-3}) following Strickland and Parsons (1972) to determine the chlorophyll-a (Chl-a) concentration. The Chl-a (mg m^{-3}) values at different depths were trapezoidally integrated to obtain water column Chl-a (mg m^{-2}). Continuous measurement of incident PAR (µmol photons m^{-2} s^{-1}) from dawn to dusk was carried out onboard using a 4π PAR sensor (QSL–2100, Biospherical Instruments Inc., USA) fitted in a well-lit (shadow-free) area on the monkey deck.

^{14}C-based productivity measurements

Water samples were collected from 5 discrete depths covering the euphotic zone and filtered through a 200-µm mesh to eliminate the grazers (zooplankton). Each sample was then enriched with 1 ml of $^{14}C[Na(^{14}H)CO_3]$ corresponding to 5 µCi per 250 ml of seawater in Nalgene bottles followed by incubation of the samples in a deck incubation tank continuously supplied with circulating surface seawater to maintain the ambient temperature (Knap et al. 1996). The samples (in duplicates) were incubated for 24 h (mostly from dawn to dusk) following standard simulated-in situ incubation technique (1994). Appropriate density filter packets were used to wrap the incubation bottles so as to simulate the light intensity at specific sampling depths (UNESCO-JGOFS 1994). At the end of the incubation, the samples were filtered onto 25 mm GF/F filters (®Whatman). Daily PP rates (mg C m^{-3} d^{-1}) were obtained following Strickland and Parsons (1972), which included quantification of disintegration activity in a

liquid scintillation counter (Wallac 1409 DSA). These daily PP rates (mg C m^{-3} day^{-1}) at each depth were trapezoidally integrated to estimate the euphotic zone-integrated PP (IPP, mg C m^{-2} day^{-1}). The PP values were normalized with corresponding Chl-a to calculate the Chl-a specific PP (P^B) (mg C (mgChl-a)$^{-1}$ day^{-1}), which is an index for phytoplankton physiological adaptation to the ambient environment (Behrenfeld and Falkowski 1997a, b).

Relationship between P^B at discrete depths and corresponding underwater PAR (PAR–P^B relationship) was deduced using curve fitting method. Here, the PAR–P^B relationship does not represent the true photosynthesis-irradiance (P–E) response of the phytoplankton assemblages but represents the relation between P^B and corresponding PAR at discrete depths within the water column (Sakshaug et al. 1997; Tripathy et al. 2010) For the stations where photoinhibition was evident, the P–E model developed by Steele et al. (1962) was used, which can be expressed as hereunder:

$$P^B = P^B_{opt}\left(E/E_{max}\right) - \exp\left[1 - \left(E/E_{max}\right)\right] \quad (1)$$

where, P^B, P^B_{opt} and E_{max} are rates of Chl-a normalized carbon fixation (mgC (mg Chl-a)$^{-1}$ h^{-1}), Chl-a normalized optimal carbon fixation in the water column (mgC (mg Chl-a)$^{-1}$ h^{-1}) and irradiance value at inflection point between light-saturated and light-limited phases (µE m^{-2} s^{-1}), respectively.

In case of absence of photoinhibition, the curve fitting was carried out using the Webb et al. (1974) equation described hereunder

$$P^B = P^B_{opt}\left[1 - \exp\left(-E/E_{max}\right)\right] \quad (2)$$

The photosynthetic parameters for Eq. (2) are same as those defined for Eq. (1). Acronyms and abbreviations used in this study are listed in the Table 1.

Fast repetition rate fluorometry-based measurements

Profiling of a Fast Repetition Rate fluorometer (FRRf; FastOcean APD, CTG Ltd., UK) was carried out at a vertical rate ≤ 0.5 m s^{-1} to provide adequate interrogation of the phytoplankton within the water column to obtain high resolution data on phytoplankton physiological properties like maximum photochemical efficiency of photosystem II at dark (F_v/F_m) and light $\left(F'_q/F'_m\right)$, functional absorption cross-section of photosystem II at dark (σ_{PSII}) and light $\left(\sigma'_{PSII}\right)$ condition, reaction centre concentration (RCII), etc., at approximately 1 m interval in the water column. The Non-photochemical Quenching (NPQ_{NSV}) of fluorescence was measured following Oxborough et al. (2012). The excitation and relaxation protocols were set for 450, 530 and 624 nm as per the manual provided by CTG, UK. The vessel was re-orientated to avoid ship shadow prior to each FRRf cast. All FRRf parameters were obtained under ambient plus dark (APD) conditions.

Absorption coefficients of phytoplankton and non-phytoplankton particles

Water samples from different depths of the euphotic zone were analysed to obtain phytoplankton absorption (a_{ph}) following Mitchell et al. (1990). 1 l of water sample from each depth was filtered separately onto a 25 mm GF/F (0.7 µm) paper under a low suction pressure. The residues on filter papers were measured within 400–700 nm wavelength at 1 nm interval using a UV–Vis 2600 spectrophotometer (Shimadzu, Japan) with an integrating sphere. The path-length amplification effect of the glass fibre filter caused due to multiple scattering was corrected using the equation proposed by Cleveland and Weidemann (1993):

$$OD_s(\lambda) = 0.378OD_f(\lambda) + 0.523OD_f(\lambda)^2 \quad (3)$$

where $OD_s(\lambda)$ and $OD_f(\lambda)$ are optical density (OD) of the particulate matter in suspension and filter, respectively. Absorption coefficient of the total particles present in suspension ($a_p(\lambda)$) was calculated using the equation:

$$a_p(\lambda) = 2.303OD_s(\lambda) * S/V \quad (4)$$

where 2.303 = conversion factor for $\log_{10}$ to $\log_e$, S = clearance area measured for the filter paper (m^2), V = filtered volume (ml), S/V = approximate geometrical light path-length.

After measuring OD for particulate matter, the filter papers were soaked in absolute methanol for 24 h to extract the phytoplankton pigments. After rinsing with Filtered Sea Water (FSW), absorbance of the decolourized papers were re-measured to obtain OD of the non-phytoplankton particles ($a_{nph}(\lambda)$) following Kishino et al. (1985). Using Eq. (4) $a_{nph}(\lambda)$ was calculated. The absorption coefficient of phytoplankton ($a_{ph}(\lambda)$) was obtained by substituting $a_{nph}(\lambda)$ from $a_p(\lambda)$ as follows:

$$a_{ph}(\lambda) = a_p(\lambda) - a_{nph}(\lambda) \quad (5)$$

The averages of duplicate spectra were used in this study. The a_{ph} values were normalized by Chl-a to determine chlorophyll-specific phytoplankton absorption coefficients ($a^*_{ph}(\lambda)$).

Absorption coefficients of chromophoric dissolved organic matter

The light absorption coefficient for Chromophoric Dissolved Organic Matter (a_{CDOM}) was measured by filtering

Table 1 List of acronyms and abbreviations used

Abbreviation	Description	Unit
CDOM	Chromophoric dissolved organic matter	
Chl-a	Concentration of chlorophyll-a	mg m^{-3}
Chl_{int}	Water column-integrated Chl-a	mg m^{-2}
DCM	Deep chlorophyll maximum	
MLD	Mixed layer depth	m
AOP	Apparent optical properties	
IPP	Integrated primary production in the euphotic zone	mgC m^{-2} day^{-1}
PP	Primary Productivity	mgC m^{-3} day^{-1}
P^B	Chl-a normalized primary productivity	mgC mgChl-a^{-1} day^{-1}
P^B_{opt}	Maximum P^B in the water column	mgC mgChl-a^{-1} day^{-1}
Z_{eu}	Depth of the euphotic zone	m
PAR	Photosynthetically active radiation	µEinstein m^{-2} s^{-1}
K_d	Diffuse attenuation coefficient of PAR	m^{-1}
SST	Sea surface temperature	°C
TSM	Total suspended matter	mg l^{-1}
VGPM	Vertically generalized production model	
FRRF	Fast rate repetition fluorometry	
PS II	Photosystem II	
F_v/F_m	Maximum photochemical efficiency of PS II	Dimensionless
F'_q/F'_m	Effective photochemical efficiency of PS II	Dimensionless
σ_{PSII}	Functional absorption cross-section of PS II in dark	nm^{-2}
σ'_{PSII}	Functional absorption cross-section of PS II in light	nm^{-2}
a_{tot}	Total absorption coefficient, $a_{tot}=a_{ph}+a_{nph}+a_w$	m^{-1}
a_{CDOM}	Absorption by CDOM	m^{-1}
a_{nph}	Absorption by non-phytoplankton particles	m^{-1}
a^*_{ph}	Chl-a specific absorption coefficient	m^{-2} mg Chl-a^{-1}
a_{ph}	Absorption by the phytoplankton	m^{-1}
a^*_{sol}	Specific absorption coefficient of Chl-a ideally dispersed in solution	m^{-2} mg Chl-a^{-1}
a_w	Absorption by pure water	m^{-1}
E_d	Spectral downwelling irradiance	mW cm^{-2} nm^{-1}
L_w	Water-leaving radiance	mW cm^{-2} nm^{-1} sr^{-1}
R_{rs}	Remote sensing reflectance $R_{rs}=L_w/E_d$	sr^{-1}
λ	Wavelength	nm
Q^*_a	a^*_{ph}/a^*_{sol}(indicator of the pigment packaging)	Dimensionless

the subsamples through 47 mm GF/F (Whatman) to eliminate the larger particles. The samples were once again filtered through 47 mm Nucleopore filters (pore size: 0.2 µm) to remove the smaller particles. Both the filters were rinsed with Milli-Q water before filtration. The filtrates were stored in dark condition for a few hours in order to attain equilibrium to room temperature. The absorption measurements were performed by spectrophotometer with an integrating sphere (UV–Vis 2600, Shimadzu, Japan) using a 10 cm path-length quartz cuvette and Milli-Q water as reference. The normalization of absorbance was done to zero at 600 nm to eradicate temperature-dependent interferences observed between 650 and 750 nm. Blank values (Mill-Q water) were subtracted from every wavelength in the spectrum (Mitchell et al. 2002). The following equation was used in order to determine the a_{CDOM} at every station:

$$a_{CDOM}(\lambda) = \frac{2.303}{l}\left[\left\{OD_s(\lambda) - OD_{fsw}(\lambda)\right\} - OD_{null}\right] \quad (6)$$

where $OD_{s,\ fsw}$ and $_{null}$ are the optical densities of sample, purified filtered sea water, and at null absorption wavelength. The optical path-length, l=0.1 m = 10 cm and a_{CDOM} is expressed in m^{-1}. The total absorption coefficient (a_{tot}) value was then calculated by summing up the values obtained for a_p, a_{CDOM} and a_w (absorption by pure water) at specific wavelengths and sampling depths. The values for a_w were obtained from Pope and Fry (1997).

Estimation of total suspended matter

Water samples from two depths (surface and DCM) collected at each station were processed to determine the concentration of total suspended matter (TSM). The samples were filtered through prewashed and pre-weighed (w_1) 47 mm Millipore filters (pore size 0.45 µm) under a low vacuum pressure (approx. 120 mmHg). The filters were then oven dried at 60℃ for 4 h and re-weighed to obtain the final weight (w_2). The concentration of TSM for each station was expressed in mg l^{-1}.

$$\text{TSM}\left(\text{mg l}^{-1}\right) = \left(w_2 - w_1\right)/(V * 0.001) \quad (7)$$

where V = the volume of water filtered (L).

Hyperspectral radiometric measurements

A hyperspectral optical profiler (HyperProII, Satlantic, Canada) was deployed in free-fall profiling mode to record the apparent optical properties (AOP) in the euphotic zone. This instrument provides information about the downwelling irradiance (E_d), upwelling radiance (L_u), remote sensing reflectance (R_{rs}), diffuse attenuation coefficient of PAR (K_d) at 1 nm interval from 354 to 800 nm. Care was taken to avoid shade and ship induced disturbances (vibrations) while deploying the instrument. The optical profiler data were processed by ProSoft software package and downward cast data were considered for interpretation. Derivation of total absorption ($a_{ph}+a_{nph}+a_{CDOM}$) by inversion of the spectral R_{rs} was carried out following the quasi-analytical algorithm (QAA, v4) with optimization technique (Lee et al. 2002). Ocean chlorophyll (OC) algorithms version OC2, OC3 and OC4 were used to retrieve modelled Chl-a from the radiometric-based R_{rs} so as to compare the same with its in situ counterpart.

Satellite-based primary productivity

The euphotic depth (Z_{eu}, the depth where PAR reduces to 1% of its value just beneath the surface) integrated PP (IPP) was estimated from the satellite-derived variables using the vertically generalized production model (VGPM) proposed by Behrenfeld and Falkowski (1997b). The VGPM is expressed as follows:

$$\text{IPP} = 0.66125 \times P^B_{\text{opt}} \times \left[E_0/\left(E_0 + 4.1\right)\right] \times Z_{eu} \times \text{Chl}_0 \times DL \quad (8)$$

where IPP, P^B_{opt}, E_0, Z_{eu}, Chl_0 and DL are euphotic zone-integrated daily PP (mgC m^{-2} day^{-1}), Chl-a normalized maximum PP in the water column (mgC mgChl-a^{-1} h^{-1}), PAR value at sea surface (E m^{-2} day^{-1}), depth of the euphotic zone estimated from sea surface Chl-a (Chl_0) according to Morel and Berthon (1989), sea surface Chl-a (mg m^{-3}), and daylength (in hours) calculated following Kirk (1994), respectively. The light-dependent function $[(0.66125E_0)/(E_0+4.1)]$ describes the relative change in the light saturation fraction of the Z_{eu} as a function of E_0. The P^B_{opt} is expressed as the 7th order polynomial function of SST (Behrenfeld and Falkowski 1997b). Daily SST was obtained from AVHRR, whereas daily PAR and weekly Chl-a (since daily values are not available) was retrieved from MODIS-AQUA sensors (https://oceancolor.gsfc.nasa.gov/l3/) with a spatial resolution of 4×4 km from the data provided by NASA. Daylength varied from 14 to 16 h during the sampling period.

Results

Hydrographical characteristics

The hydrographical characteristics in the upper 120 m of the four frontal regions were quite different from each other. Vertical profiles of temperature (Fig. 2a) showed the least mean value at PF2b (1.71 ± 0.57 °C) and maximum (15.75 ± 1.91 °C) at STF. Salinity profiles (Fig. 2b) showed lowest mean value at STF (33.80 ± 0.54) and highest mean value at PF2a (33.92 ± 0.58). The SST increased from PF2a towards STF (2.4–18.8 °C), whereas the sea surface salinity (SSS) was lowest (33.75) at STF and highest (34.30) at SAF (Table 2). The variation of temperature was more pronounced in the water column than salinity variations among the fronts. However, sharp variation in salinity in the surface layers (< 10 m) at SAF and PF2 was observed. The mixed layer depth (MLD) was deepest at PF2 followed by PF1 and SAF, whereas STF showed no clear mixed layer. The estimated N (Fig. 2c) showed a weaker stability (negative values) in the PF2 and PF1 which indicated the weaker stratification in this region during the observation. However, stronger N (positive values) in the SAF and STF indicated that the region was more stratified than PF. In general, upper water column (upper 40 m) of the study region was well mixed during the study. The DO profile (Fig. 2d) showed highest mean values at PF2a (7.53 ± 0.20 ml l^{-1}) and the least at STF (6.83 ± 0.08 ml l^{-1}). Vertical distribution of DO was nearly homogenous at all the stations. However, like salinity profiles, sharp fluctuations were observed at PF2 and SAF within the upper 10 m.

The vertical distribution of PAR (Fig. 2e) is primarily dependent on not only the surface incoming PAR but also the diffuse attenuation coefficient of PAR (K_d). The vertical profile of PAR showed a typical exponential decrease with highest PAR observed at PF2a (142.83 µmol photons

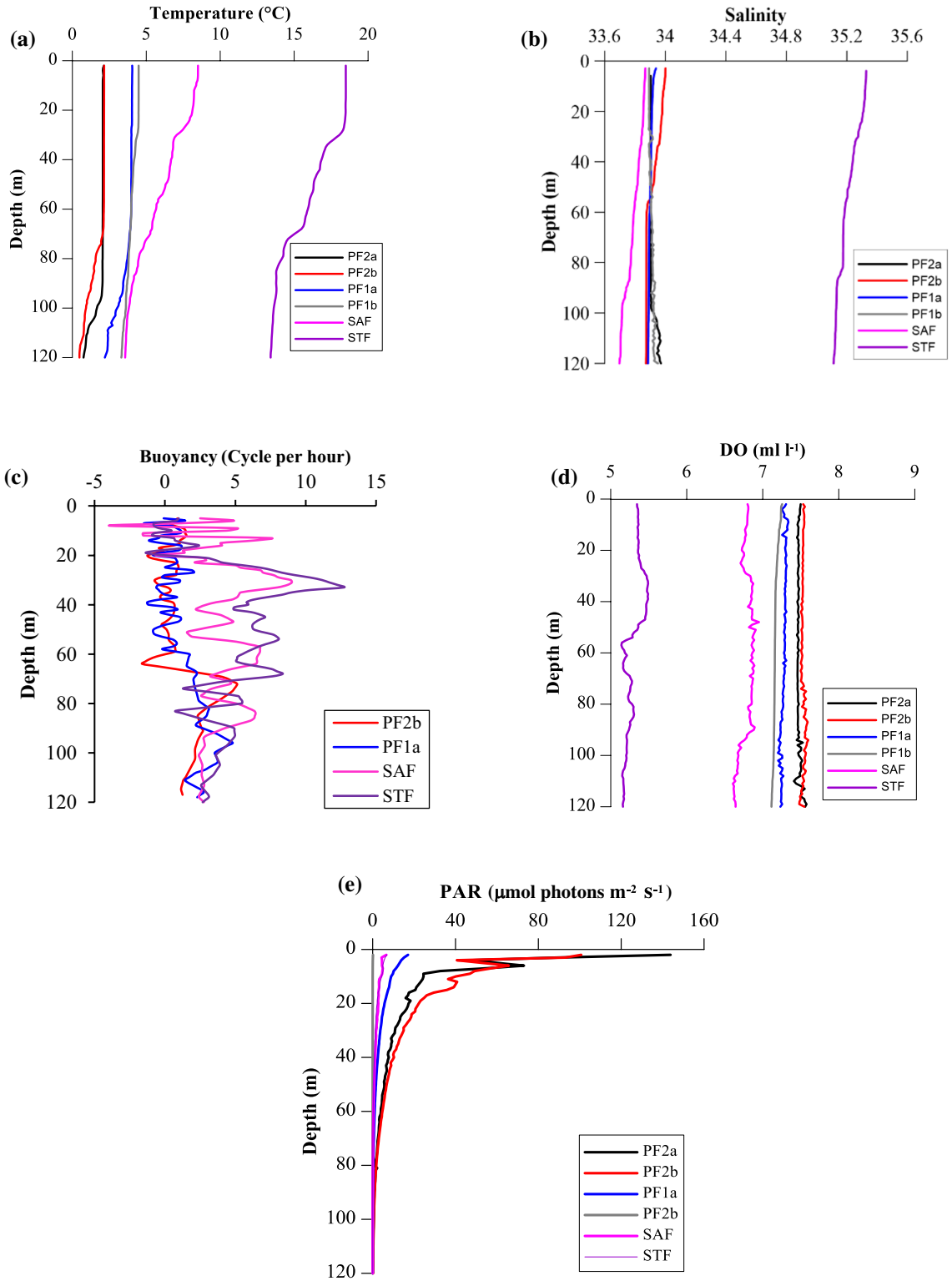

Fig. 2 Vertical profiles of in situ temperature (**a**), salinity (**b**), buoyancy frequency (of the four representative fronts) (**c**), dissolved oxygen (**d**) and PAR (e) measured by CTD at different frontal locations

Table 2 Station number, frontal zones, latitude, longitude, sea surface temperature (SST), sea surface salinity (SSS), surface nutrients (NO_3, SiO_4, PO_4), water column average N:P and N:Si ratios, surface dissolved oxygen (DO), daily incident photosynthetically active radiation (PAR), surface Chl-a (Chl_0), column-integrated Chl-a (Chl_{int}), surface primary productivity (Sur. PP), column-integrated PP (IPP), and surface Chl-a specific PP (P^B) in the study area

Stations	Fronts	Lat (°S)	Date of sampling	Long (°E)	SST (°C)	SSS	NO_3 (μM)	SiO_4 (μM)	PO_4 (μM)	N:P	N:Si	DO (ml l^{-1})	PAR (E m^{-2} day^{-1})	Chl_0 (mg m^{-3})	Ch_{int} (mg m^{-2})	Sur. PP (mgC m^{-3} day^{-1})	IPP (mgCm^{-2} d^{-1})	P^B (mgC (mgChl-a)$^{-1}$ day^{-1})
1	STF	42.60	16-Feb	57.50	18.5	33.75	3.5	6.59	0.75	5.0	0.58	5.34	41.65	0.26	35.95	3.34	258.58	7.19
2	SAF	46.47	11-Feb	57.52	8.5	34.30	22.39	6.61	1.85	12.9	4.02	6.80	26.66	0.25	29.65	3.72	237.53	8.01
3	PF1a	51.62	10-Feb	51.50	4.0	33.91	23.68	8.82	1.75	14.1	2.88	7.30	53.15	0.11	25.50	1.86	224.29	8.79
4	PF1b	51.02	09-Feb	57.47	4.5	33.93	23.84	14.09	2.08	12.2	2.16	7.26	31.51	ND	ND	2.04	236.97	ND
5	PF2b	55.48	07-Feb	51.52	2.2	33.90	26.44	26.30	2.00	13.4	1.05	7.50	59.84	0.11	23.52	1.60	188.28	8.01
6	PF2a	55.55	05-Feb	55.50	2.1	34.02	27.11	26.39	2.00	13.8	1.06	7.49	49.27	0.13	18.82	1.26	193.13	10.26

ND no data

m^{-2} s^{-1}) and lowest at SAF (0.15 μmol photons m^{-2} s^{-1}). This variation can be linked to the time of CTD deployment which differed from station to station. Furthermore, low PAR due to presence of cloud cover cannot be ruled out.

Nutrients distribution

The vertical profiles of nutrients showed marked variation among the fronts. NO_3 (Fig. 3a) concentrations were homogeneous in the water column (120 m) for PF stations. However, it increased at SAF below MLD, and a gradual increase with depth was noticed for STF indicating probable upwelling of nutrient-rich waters from deep below. Similar trend was exhibited for PO_4 (Fig. 3b). But SiO_4 values showed a clear increase after the MLD (Fig. 3c) with PF2 depicting distinctly higher concentrations among fronts. On the other hand, the STF was typified by least NO_3 and PO_4 values. The macronutrients showed a north–south increasing gradient (Table 2), as least concentrations of NO_3 (3.50 (μM)), PO_4 (0.75 (μM)) and SiO_4 (6.59 (μM)) were observed at STF, whereas PF2a was characterized by the highest concentrations of NO_3 (26.44 (μM)), PO_4 (2.00 (μM)) and SiO_4 (26.39 (μM)). Analysis of nutrient ratios in the study area indicated highest N:P (13.40), N:Si (1.06) and Si:P (13.12) at PF2 stations (Table 2). PF1a and PF1b also exhibited high N:P (14.13 and 12.17) and N:Si (2.88 and 2.16) but low Si:P (5.15 and 6.72) values. High N:Si (4.02) and low Si:P (3.53) were observed at SAF while the STF corresponded to the least N:P (5.0), N:Si (0.58) and a low Si:P (8.84) ratio.

Chl-a, ^{14}C-based primary productivity and PAR–P^B relationship

The surface Chl-a (Chl_0) concentrations varied from 0.11 (PF2b) to 0.26 mg m^{-3} (STF) during the study period indicating higher Chl_0 at the stations to the north of PF (Table 2). The Chl-a profiles (Fig. 4a) showed low values at surface and distinct DCM. Similar to Chl-a, the vertical PP profiles showed low surface and higher subsurface values (Fig. 4b) and the depths of PP maxima at each front were shallower than the corresponding DCM depths. A weak relationship was observed between the Chl-a and PP at discrete depths in the water column ($R^2 = 0.32$, $p < 0.05$; Fig. 4c); however, their depth-integrated values were significantly correlated ($R^2 = 0.86$, $p < 0.001$; Fig. 4d).

The daily integrated incident PAR (E_0) varied from 26.66 mol photons m^{-2} day^{-1} (at SAF) to 59.84 mol photons m^{-2} day^{-1} (at PF2b) during the observation period with no trend in daily PAR variability across the fronts. STF showed maximum PP despite the least observed PAR. Uniform values of P^B (Chl-a specific PP) were observed at all the stations. The PAR–P^B relationships for STF, SAF and PF1 was

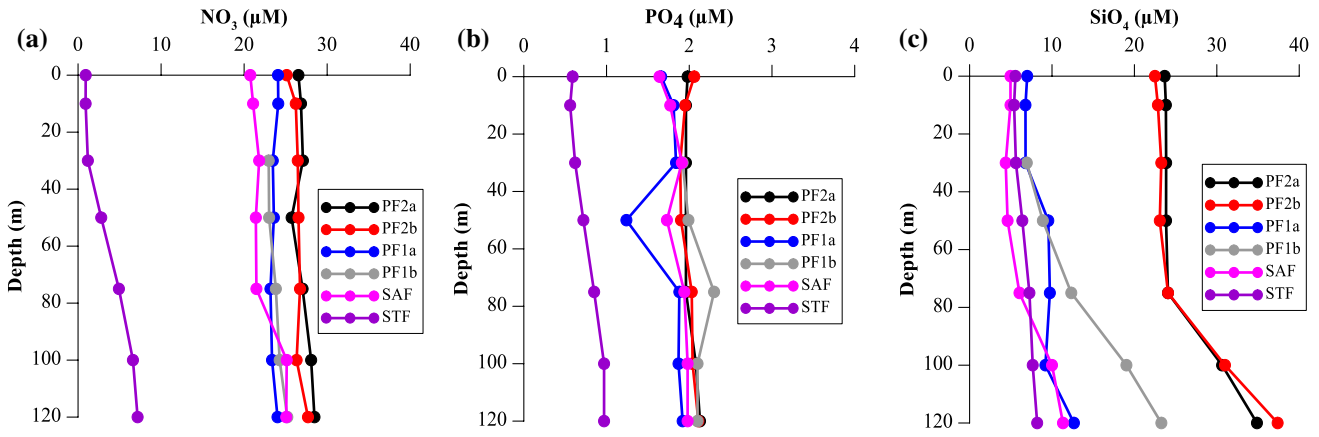

Fig. 3 Vertical distribution of nitrate (**a**), phosphate (**b**), and silicate (**c**) at different frontal regions

linear (Fig. 4e), whereas for PF2 stations it was curvilinear (Fig. 4f).

Satellite-based observations

Satellite-derived and in situ daily integrated PAR were strongly correlated ($R^2 = 0.87$, $p < 0.01$), but satellite PAR was underestimated at all stations (Fig. 5a) except at the PF. In situ and remotely sensed Chl-a in the PF region were close to 1:1 line; however, satellite measurements underestimated at SAF and STF. VGPM-based IPP varied from 173.12 to 473.55 mgC m^{-2} day^{-1}. The in situ IPP strongly correlated with the VGPM-based IPP accounting for 94% ($R^2 = 0.94$, $RMSE = 77.48$, $p < 0.01$) of the observed variability in it (Fig. 5b). IPP values at PF2 were almost on 1:1 line, whereas values at PF1 were closer to this line. However, the VGPM-IPP overestimated (1.2 times) the measured IPP at SAF and STF stations.

Photosynthetic parameters from Fast Repetition Rate fluorometry

The maximum (F_v/F_m) and effective $\left(F'_q/F'_m\right)$ photochemical efficiency of PSII in the study area varied from 0.09 to 0.42 (avg. 0.32 ± 0.06) and 0.11 to 0.48 (avg. 0.31 ± 0.07), respectively. F_v/F_m and F'_q/F'_m was the least at PF1, whereas highest at STF (Fig. 6a–b). Similar trend was also observed for functional absorption cross-section in darkness (σ_{PSII}) and under ambient light $\left(\sigma'_{PSII}\right)$ condition (Fig. 6c–d), which varied from 1.38 to 8.35 (avg. 4.93 ± 1.31) and 1.14 to 7.92 (avg. 5.08 ± 1.34) nm^2 $PSII^{-1}$, respectively. The vertical profile of F_v/F_m and F'_q/F'_m was low at surface layers, increased with depth, attained maximum values (indicating healthier phytoplankton) in the subsurface layers (> 60 m) and thereafter similar values were maintained at deeper depths except at STF where a clear decrease in photochemical efficiency values was observed after 80 m. Subsurface maxima for F_v/F_m values were observed at all the stations, which nearly coincided with the Chl-a and fluorescence profiles. A decrease in F_v/F_m below the DCM layer, where Chl-a concentrations started to decrease, was often observed (Fig. 6a). Due to instrumental error, the surface values for F'_q/F'_m and σ'_{PSII} could not be recorded (Fig. 6b–d), but from the distribution pattern at subsurface layers it can be presumed that fluorescence quenching at surface layer was stronger at PF1 and PF2 than STF (Fig. 6e–f). Average non-photochemical quenching (NPQ_{NSV}) values of 0.59 at PF2a, 9.64 at PF2b, 2.53 at PF1b, 1.01 at PF1a, 1.02 at SAF and 2.05 at STF, respectively, were observed during the study.

Characteristics of the bio-optical variables

The measured a_{ph} spectra (Fig. 7a, b) were characterized by the presence of absorption peaks at 440, 490 and 675 nm. Mean values of both a_{ph} and a^*_{ph} were similar with slightly higher values at surface than at DCM (Fig. 7a, d). Surface a_{ph} (443) values was highest at PF2a (0.067 m^{-1}) and lowest at PF1a (0.006 m^{-1}), whereas for DCM it was maximum at STF (0.060 m^{-1}) and minimum at PF2a (0.010 m^{-1}). Similarly, surface a^*_{ph} (443) values were also highest at PF2a (0.511 m^{-1}) but lowest at PF1a (0.062 m^{-1}), for DCM it was also maximum at STF (0.213 m^{-1}) but minimum at SAF (0.074 m^{-1}) (data not shown). The CDOM absorption values ranged from 0.0045 to 1.304 m^{-1}. The concentration of TSM ranged between 4.8 and 6.0 mg l^{-1} at the surface and from 3.6 to 5.6 mg l^{-1} at the DCM.

To quantify the relative contributions (%) of surface a_{ph}, a_{nph} and a_{CDOM} to the total non-water absorption, a ternary diagram displaying the absorption coefficients' corresponding to waveband 443 nm was plotted (Fig. 8). The

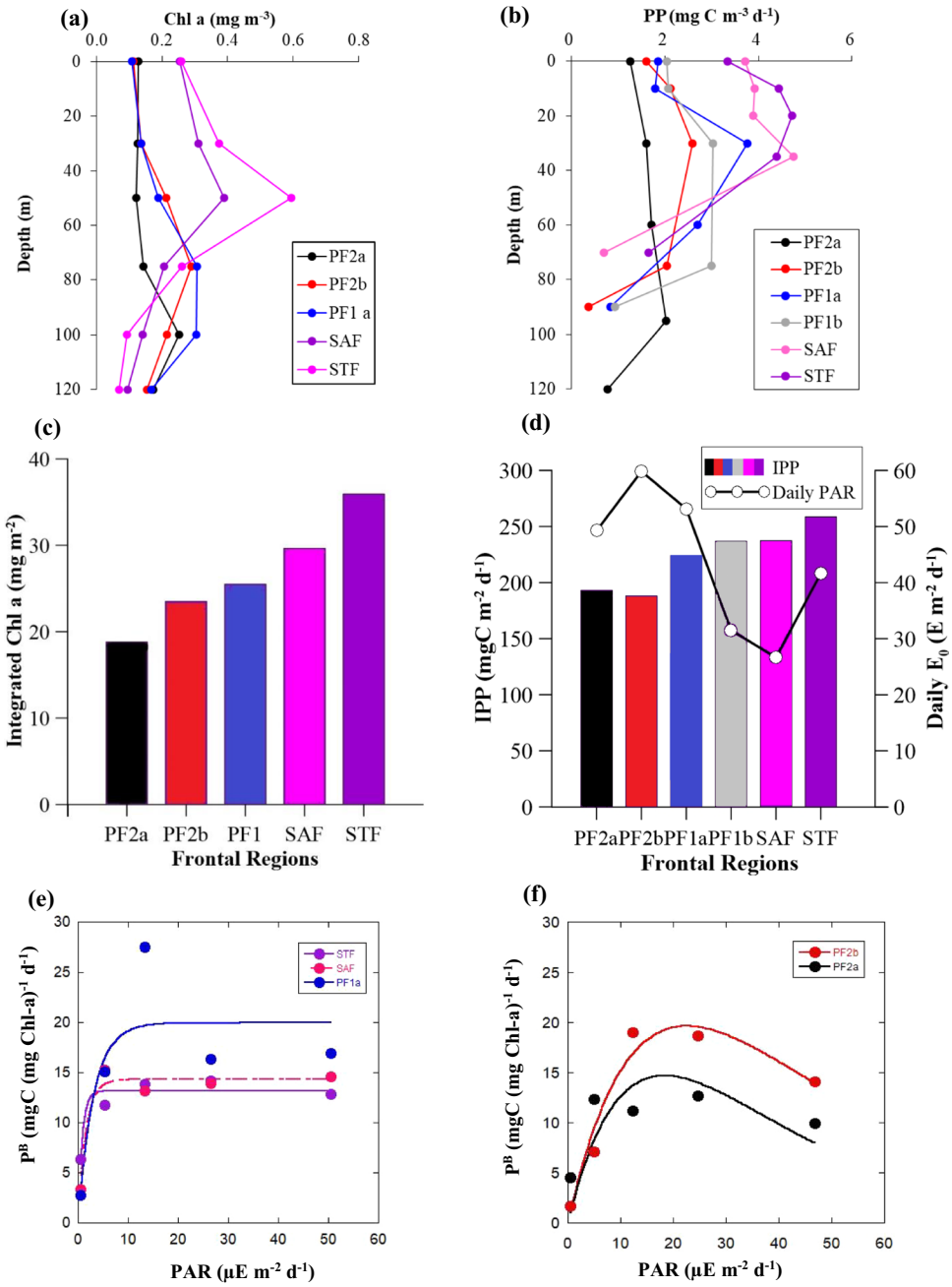

Fig. 4 Vertical profiles of chlorophyll-a (**a**), ^{14}C-based primary productivity (**b**), water column-integrated chlorophyll-a (**c**), primary productivity (**d**), and daily incident PAR and Daily PAR–P^B relationships in the water column at different sampling locations (**e**, **f**)

surface a_{CDOM}, a_{nph} and a_{ph} exhibited clear variations in the study area ranging from 0.30 (PF1a)–0.91 m^{-1} (STF), 0.03 (PF2a)–0.61 m^{-1} (PF1a) and 0.008 (PF1a)–0.10 m^{-1} (STF), respectively. Chl-a was strongly correlated to a_{ph} (443), a_{ph} (676) and moderately to a_p (676) with R^2 values of 0.72 ($p < 0.05$), 0.64 ($p < 0.05$) and 0.45, respectively, in the water column (Fig. 9a–c). The a_p (443) showed a moderate relation ($R^2 = 0.40$) with a_{ph} (443) but did not show any significant relationship with Chl-a (not shown). The ratio of a_{nph} to a_p at 443 nm was inversely related with Chl-a (Fig. 9d). Chl-a was positively correlated to a_{CDOM} (440) and a_{CDOM} (412) with R^2 values of 0.31 and 0.33, respectively (Fig. 9e, f). TSM showed an inverse relationship ($R^2 = 0.55$) with Chl-a (Fig. 9g) indicating that the surface layer had higher concentration of TSM than DCM where phytoplankton biomass was higher. Furthermore, it showed a positive relation ($R^2 = 0.55$) with a_{CDOM} (Fig. 9h) and a negative correlation with temperature both at surface ($R^2 = 0.30$) and at DCM ($R^2 = 0.42$). The relationship of TSM with salinity was weakly negative at surface ($R^2 = 0.26$) and moderately positive at DCM ($R^2 = 0.56$). A positive relationship ($R^2 = 0.41$) was observed between a_{CDOM} and water temperature.

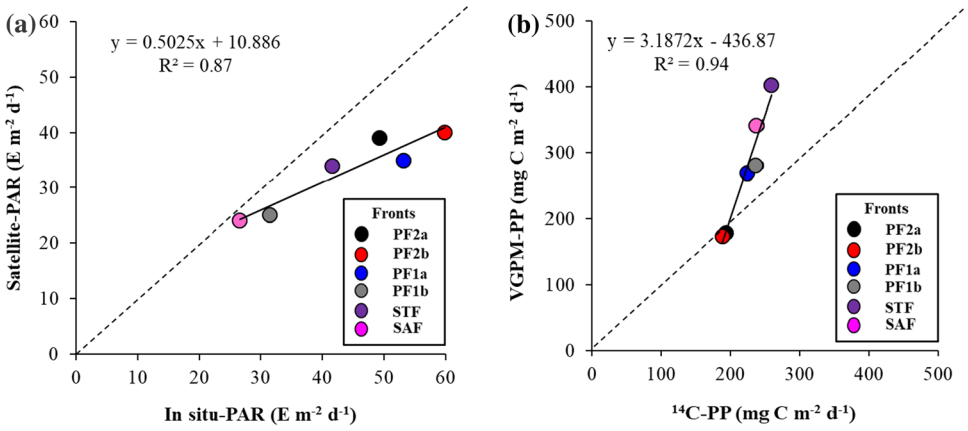

Fig. 5 Scatter plots showing comparisons of in situ and satellite-based daily incident surface PAR (**a**) and daily primary productivity (**b**) at the sampling locations

The a^*_{ph} (676), a good indicator of package effect in phytoplankton (Alcantara et al. 2016) showed positive significant relationship (no package effect) with Chl-a at surface ($R^2 = 0.95$, $p < 0.01$) and weak inverse relationship (presence of package effect) at DCM ($R^2 = 0.33$, $p < 0.05$) except at STF. The a^*_{ph} at 443 and 676 nm were positively correlated ($R^2 = 0.68$, $p < 0.05$) (Fig. 10a) and the ratio of a^*_{ph} at 443 and 676 nm showed significant correlation ($R^2 = 0.74$, $p < 0.05$) with incident surface PAR (Fig. 10b). The blue to red ratio of a^*_{ph} in the study area varied from 3.15 to 8.81 in surface layer, i.e. the $a^*_{ph}(443)/a^*_{ph}(676)$ was > 3 for surface waters.

The dimensionless factor Q^*_a (676) is a ratio of a^*_{ph} to specific absorption coefficient of the same cellular matter ideally dispersed in solution $\left(a^*_{sol}\right)$, and is used as an indicator of pigment packaging. It was found that the specific absorption coefficient of Chl-a in solution is approximately 0.0207 $m^2\ mg^{-1}$ of Chl-a at 676 nm and hence, variations in Q^*_a at 676 nm (Q^*_a (676)) can be theoretically formulated as $Q^*_a(676) = a^*_{ph}(676)/0.0207$ (Bricaud et al. 1995). A moderate inverse relationship ($R^2 = 0.60$) was observed between Q^*_a (676) and Chl-a (Fig. 10c) and the Q^*_a (676) values ranged from 0.5 to 3.3. Surface Q^*_a (676) values were > 1 at STF (1.01), SAF (1.03) and PF1 (3.17), while they were found to be < 1 for SAF (0.80) and PF2b (0.50) at DCM.

The relationship between phytoplankton absorption with PP and hydrographic parameters were investigated. a_{ph} (676) and a^*_{ph} (676) showed moderate positive correlation (not significant) with corresponding PP resulting in R^2 values of 0.48 and 0.37, respectively (Fig. 10d, e). The phytoplankton absorption coefficient and PP showed a stronger positive relationship than Chl-a and PP ($R^2 = 0.32$). Both a_{ph} (676) and a^*_{ph} (676) did not show any significant relationship with nutrient concentrations at the surface. However, an inverse correlation between a^*_{ph} (443), a^*_{ph} (676) and NO_3 ($R^2 = 0.62$, $p < 0.05$), PO_4 ($R^2 = 0.71$, $p < 0.05$) concentrations was observed at DCM (data not shown). The a_{ph} at 443 and 676 nm was positively correlated with temperature with R^2 values of 0.58 and 0.57. Conversely, when plotted versus salinity, the a_{ph} displayed weak positive relation at the surface ($R^2 = 0.33$) but strong negative relation ($R^2 = 0.75$) at DCM (please refer Table 3 that summarizes the salient bio-optical relationships described in the above subsection).

Observations from in situ hyperspectral radiometry

Measurements obtained from in situ measurements of hyperspectral radiometry were used to understand the variability of AOPs in the study area and derive R_{rs}-based Chl-a (modelled). The ratios of in situ R_{rs} (510)/R_{rs} (555) showed significant negative ($R^2 = 0.77$, $p < 0.05$) and weak positive ($R^2 = 0.16$) linear relationship (Fig. 11a, b) between in situ Chl-a and a_{CDOM} (412) (m^{-1}). The K_d (490) was retrieved using blue to green R_{rs} band ratio. The coefficients used in this retrieval are taken from SeaWiFS (Sea-Viewing Wide Field-of-View Sensor), which worked well in the SO. The K_d (490) varied from 0.30 (PF2b) to 0.64 m^{-1} (STF) in the sampling locations and showed positive relationship with in situ Chl-a and a_{ph} (490) with R^2 values of 0.30 and 0.32, respectively (Fig. 11c, d). Conversely, Chl-a showed weak relationship with R_{rs}-based a_{nph} and a_{CDOM} (figure not shown). The modelled K_d (490) was compared with averaged depth value of in situ K_d for downwelling irradiance at same wavelength (Fig. 11e), which were significantly correlated ($R^2 = 0.71$, $p < 0.05$). The blue/red ratio (B/R), i.e. a_{ph} (440)/a_{ph} (676), which serves an index to characterize the dominant phytoplankton size in water column (Wu et al. 2007; Hirata et al. 2008) was analysed. The B/R calculated from spectrophotometric and radiometric measurements of a_{ph} varied from 1.09 to 8.93 (avg. 4.42 ± 3.0) and from 4.29 to 12.35 (avg. 7.01 ± 3.25), respectively.

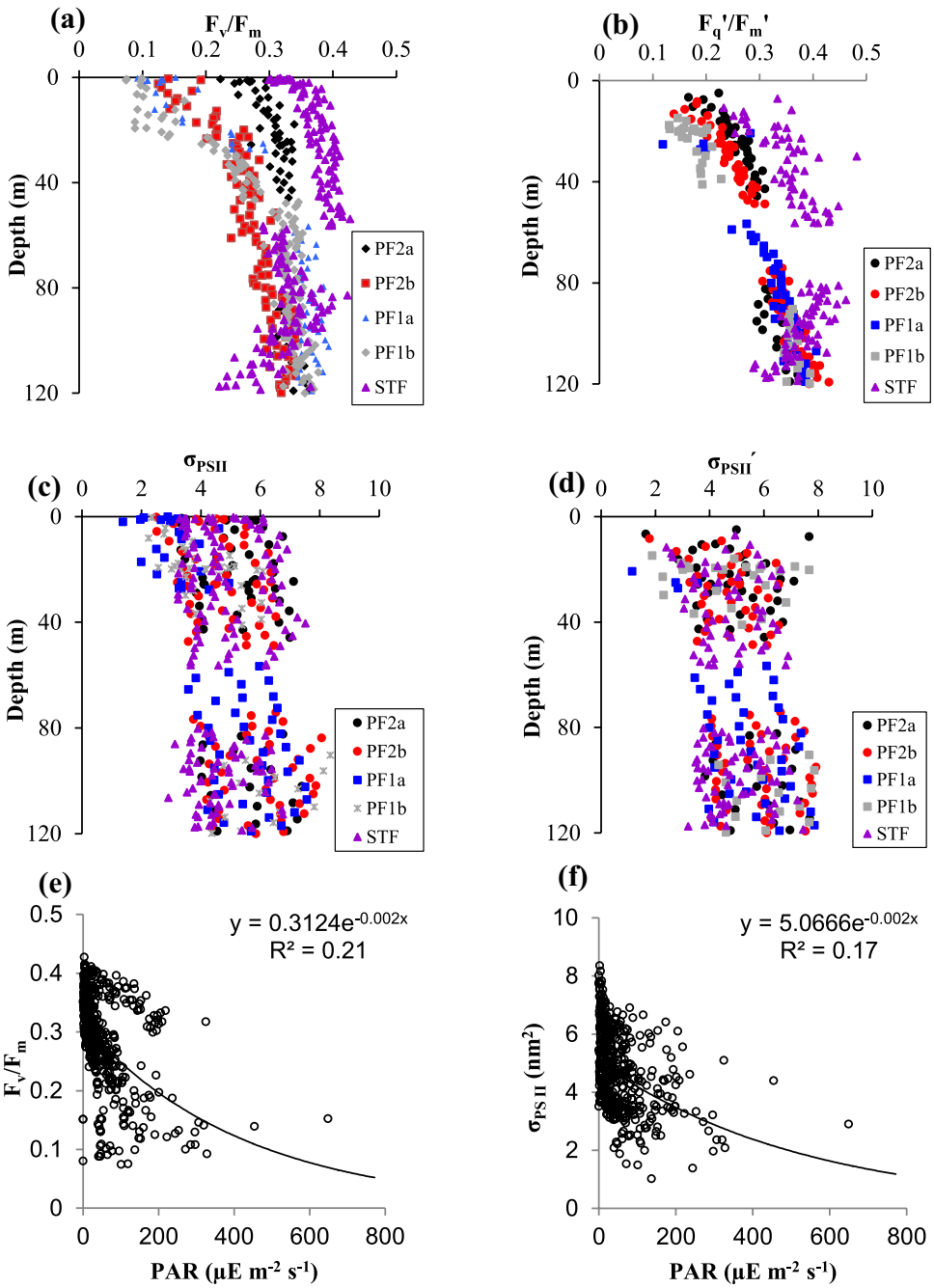

Fig. 6 Vertical profiles of F_v/F_m (**a**), F'_q/F'_m (**b**), σ_{PSII} (**c**), and σ'_{PSII} measured by FRRF (**d**); Scatter plots of ambient PAR versus F_v/F_m (**e**), and σ_{PSII} (**f**)

Discussion

Oceanographic characteristics

Large fluctuations in salinity and temperature values at SAF (in the upper 5–10 m) were well in agreement with the previous reports showing that SAF region is usually associated with the greatest temperature and salinity gradient (Holliday and Read 1998). The SST and SSS values were in par with the criteria for identifying fronts in this region (Holliday and Read 1998). Deeper MLD at PF2 indicated weaker stratification and deeper vertical mixing (as seen from the negative N values in Fig. 2) at PF, which could be attributed to the usual high wind speed prevailing in that area (Tripathy et al. 2015). The deeper mixed layer would lead to lesser light availability for phytoplankton photosynthesis and the overall metabolism (Lee et al. 2007) in these stations.

The observed nutrient concentrations are comparable to those reported previously (Jasmine et al. 2009; Gandhi et al. 2012; Tripathy et al. 2014, 2015) during austral summer. Macronutrients potentially regulate phytoplankton biomass and when their concentrations are adequate for

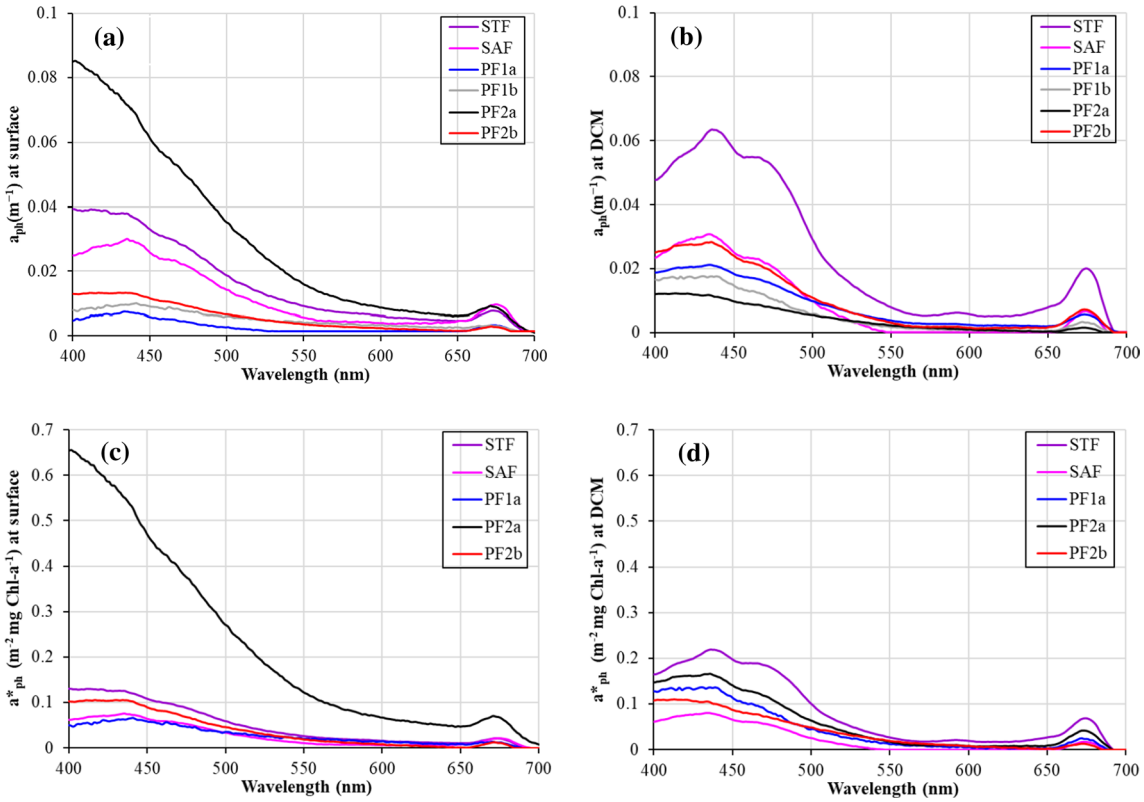

Fig. 7 Absorption by phytoplankton at surface (**a**), DCM (**b**). Chl-a specific phytoplankton absorption at surface (**c**), DCM (**d**). The solid line indicates the mean and dotted lines represent minimum and maximum values

healthy growth of diatoms, the atomic N:P:Si ratio within the cells is about 16:1:15 (Redfield 1963). These ratios have been used to study nutrient limitations in natural aquatic environments. The least N:P and low N:Si, Si:P at the STF clearly indicate NO_3 limitation (N:P ≤ 5, N:SI < 1, Levasseur and Therriault 1987) in the region. High concentrations of SiO_4 (> 10 µM) at the PF2 imply possibility of diatom dominant community in this region, whereas the regions north of PF are expected to be characterized by small and non-siliceous phytoplankton communities (Westwood et al. 2011; Tripathy et al. 2015). Nutrient ratios discerned that the ambience at SAF, PF1 was Si-limited and STF was N-limited, which was not conducive for growth of larger plankton/diatoms, whereas no nutrient limitation was apparent at PF2. Earlier findings indicate year around poor concentration of SiO_4 in the SAF region due to strong seasonal pycnocline in the SAF region (Rintoul and Trull 2001; Mendes et al. 2015). It is important to mention here that despite the HNLC conditions, phytoplankton blooms (high Chl-a) are frequently observed in surface waters over wide areas of the SO (Sabu et al. 2014; Tripathy and Jena 2019), especially where sources of iron (micronutrient) are significant. However, the concept of nutrient limitation in the present context is restricted only to the macronutrients, as measurements of iron were not carried out in the current study.

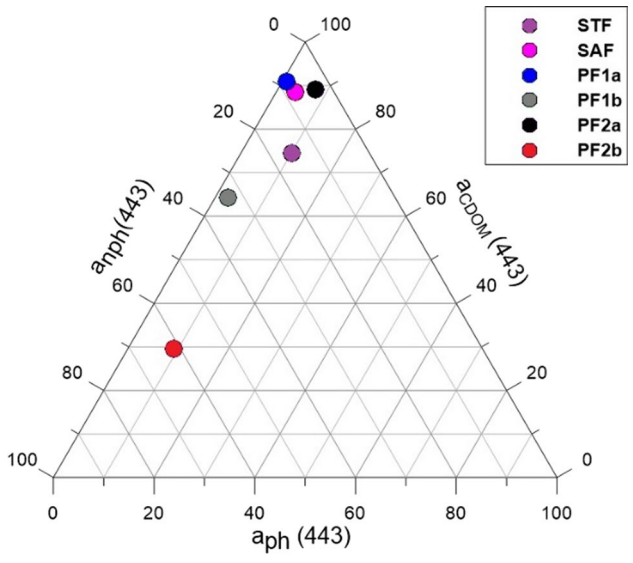

Fig. 8 Ternary plot showing % contribution of a_{ph}, a_{nph} and a_{CDOM} at 443 nm in the surface layer (~0 m) of the sampled locations

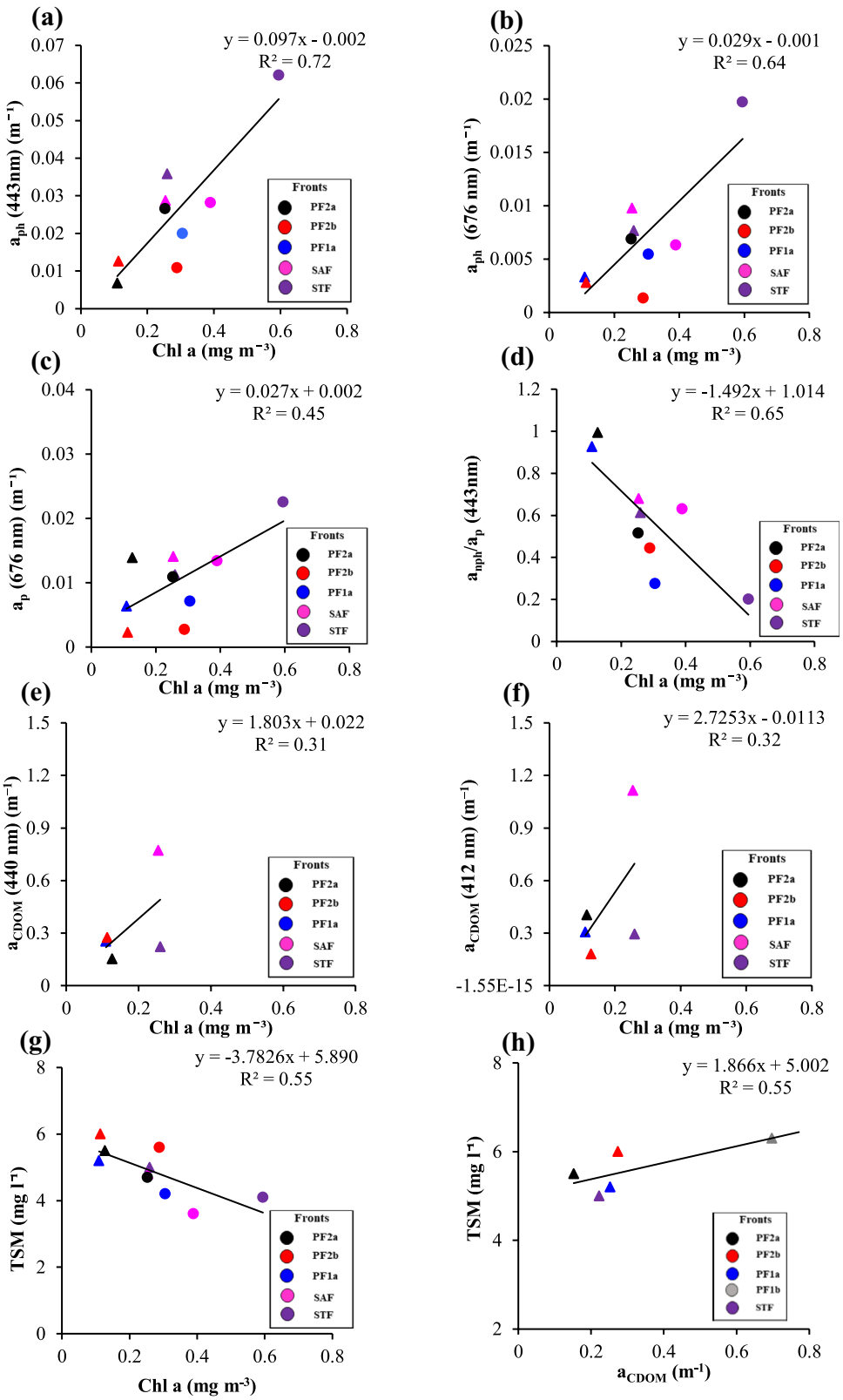

Fig. 9 Scatter plots for Chl-a and a_{ph} (443) (**a**), a_{ph} (676) (**b**), a_p (676) (**c**), a_{nph} (443)/a_p (443) (**d**), a_{CDOM} (440) (**e**), a_{CDOM}(412) (**f**) and TSM (**g**). Relationship between TSM and a_{CDOM} (**h**) in study area

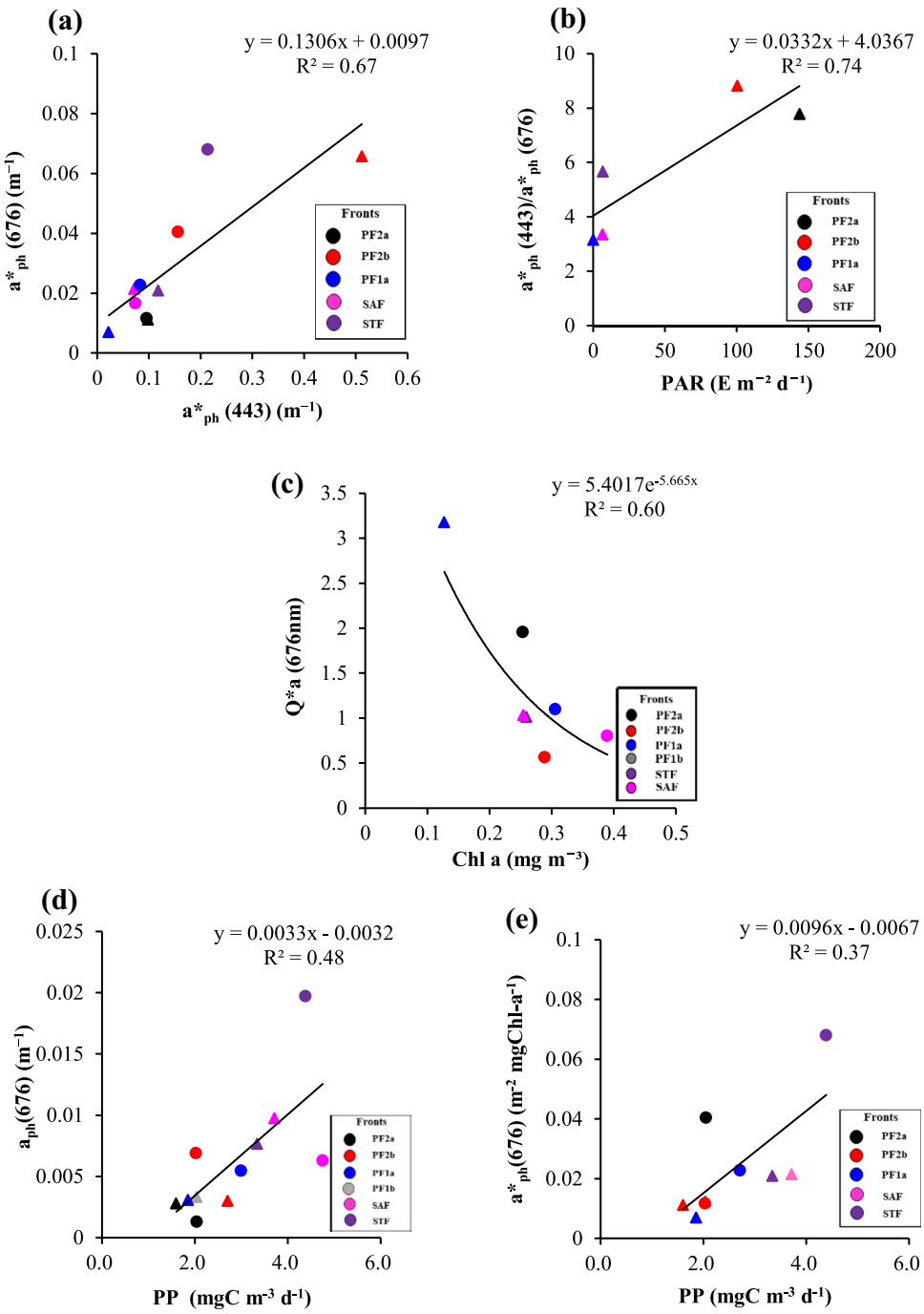

Fig. 10 Scatter plots of a^*_{ph} (676) and a^*_{ph} (443) (**a**), a^*_{ph} (443)/a^*_{ph} (676) and PAR (**b**), Q^*_a (676) and Chl-a (**c**), a_{ph}(676) vs. PP (**d**), and a^*_{ph} (676) vs. PP (**e**) in the study area

Variability in phytoplankton productivity

The productivity patterns showed a clear relation with surrounding hydrographic variables. Depths of DCM varied across fronts and deepened at PF stations compared to SAF and STF, which could be linked to the deep and shallow MLD observed at PF and northward (SAF, STF) stations, respectively. The formation, development and sustenance of DCM is governed by vertical mixing, balance of light availability and nutrient supply leading to acclimatization of phytoplankton to the ambient conditions of this region. The mismatch in depths of PP maxima and DCM could possibly be due to the interactive effects of light and nutrient limitation on phytoplankton growth (Cullen 1982). Thus, possible, active growth of photo-acclimatized phytoplankton therefore marks the DCM in the water column. We observed matching of DCM and Si-maximum, especially in the PF regions, indicating growth/accumulation of shade-adapted phytoplankton. Previous studies (Parslow et al. 2001; Gomi et al. 2010; Tripathy et al. 2015) have shown that the DCM

Table 3 Salient observations from regression analyses between: bio-optical variables and chl-a (a), physical parameters (b) and (c) inter-relationships of the bio-optical variables (the values corresponding to surface sampling layer have been italicized)

(a)	a_{ph} (443)	a_{ph} (676)	a_p (676)	a^*_{ph}(676)	a_{CDOM} (412)	TSM	a_{nph}/a_p (443)	PP
Chl-a	0.72	0.64	0.45	*0.95*, 0.33	0.32	0.55	0.65	0.32

(b)	a_{ph} (443)	a_{ph} (676)	TSM	a_{CDOM}	$a^*_{ph}(443)/a^*_{ph}(676)$	(c)	TSM	a_p (443)	a_{ph} (676)	a^*_{ph}(676)
Salinity	*0.33*, 0.75		*0.26*, 0.56			a_{CDOM}	0.55			
Temp	0.58	0.57	*0.30*, 0.42	0.41		a_{ph} (443)		0.40		
PAR					0.74	PP			0.48	0.37
						a^*_{ph}(443)				0.68

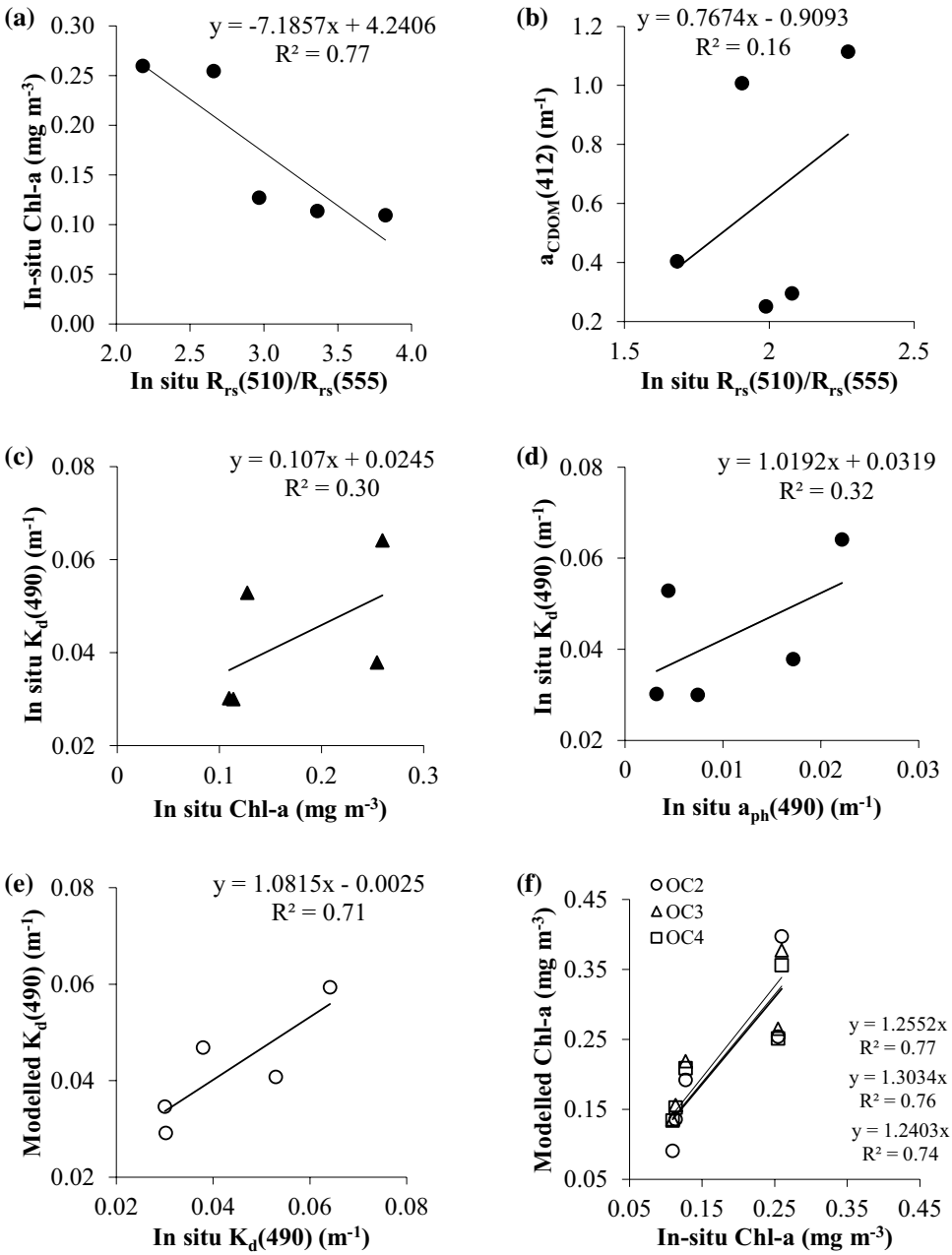

Fig. 11 Scatter plots showing chlorophyll-a as a function of ratios of R_{rs} at 510 and 555 nm (**a**), a_{CDOM} as a function of ratios of R_{rs} at 510 and 555 nm (**b**), In situ K_d (490) as a function of in situ Chl-a (**c**) and in situ a_{ph} (**d**). Comparison between in situ and modelled K_d (490) (**e**) and Chl-a (**f**) in the study area. In situ R_{rs} was derived from hyperspectral radiometry

layer (enriched with Si and Fe) was predominated by active shade-adapted flora (especially microplankton). The weak relationship between Chl-a and PP at the surface could be due to presence of senescent phytoplankton in the surface waters or stronger zooplankton grazing at surface layer than the subsurface layers (Gomi et al. 2010). The column-integrated Chl-a (Chl_{int}) was lowest at PF2a and highest at STF (Fig. 4c), which is similar to the pattern shown by Chl_0. Similar to Chl_{int}, the integrated PP (IPP) values (Fig. 4d) were lower at PF stations compared to the fronts (SAF, STF) northwards. The fronts northward to the polar fronts have been characterized by high phytoplankton biomass (Froneman et al. 1997; Graham et al. 2014). The current trend in IPP values at PF are in line with previous reports near the study area, where Jasmine et al. (2009) and Gandhi et al. (2012) have reported IPP values of 200 mgC m^{-2} day^{-1} and 215 mgC m^{-2} day^{-1}, respectively; however, the IPP observed at the STF are substantially lower than the values reported earlier (700–900 mgC m^{-2} day^{-1}). This is likely due to the observed SiO_4 and NO_3 limitation as evidenced by extremely low N:Si and Si:P ratios. Role of iron as a limiting factor for PP could not be discussed in this study due to lack of in situ data. The major causes for low PP can be attributed to the characteristic oligotrophic condition, high water column stability due to stratification and a thermocline depth deeper than the compensation depth (Jasmine et al. 2009) of the study region. A contrasting trend in IPP profiles was observed by Tripathy et al. (2015) who have reported higher IPP at PF (210.9 mgC m^{-2} day^{-1}) than at STF (152.1 mgC m^{-2} day^{-1}) and attribute it to the stronger DCM observed at PF region.

Lack of correlation between PP_{int} and integrated PAR, indicated that surface incident light did not act as a major controlling factor to modulate IPP. Earlier studies (Jasmine et al. 2009; Tripathy et al. 2014) have also highlighted an absence of any latitudinal trend in PAR variability in the study area and negated the possibility of light limitation on phytoplankton photosynthesis especially during austral summer. The similar P^B values at all the stations (except higher value at PF1) indicated less variability in photosynthetic efficiency across the fronts. The linear PAR–P^B relationship indicated no photoinhibition at the STF, SAF and PF1, whereas a curvilinear relationship indicated clear photoinhibition (decrease in surface P^B) at PF2. The absence of photoinhibition can be explained by the Si limitation at SAF, PF1 and N limitation at STF, which is favourable for the growth of smaller phytoplankton that are less susceptible to pigment package effect (discussed in the later section). Nutrient replete conditions at PF2 could be an indicator of presence of larger phytoplankton (prone to pigment packaging) in the region. Observations from satellite data were subject to overcast sky at the time of sampling as evidenced by lack of any clear latitudinal trend. The underestimation in satellite PAR was more towards higher latitudes (PF stations), where the probabilities of cloudy sky condition is usually higher. Since polar-orbiting satellite sensors (such as MODIS) observe an area on the surface of the Earth only a few times every day and measurements were interpolated using the relationship between atmospheric transmissivity and the reflectivity at the top of the atmosphere; there are high chances that the patchy cloudy sky at the time of satellite pass can lead to estimation error. Furthermore, this error could worsen by the daylength and the number of overpass counts per day in any particular area (Wang et al. 2010). Comparatively lower (at STF, SAF, PF1b) and higher (at PF2) values of daily PAR could be linked to presence and absence of overcast sky condition during the sampling time, respectively (Jasmine et al. 2009; Tripathy et al. 2014).

Similar to in situ observation, the satellite-based IPP showed that STF was the highest productive zone followed by SAF, whereas PF2 was the least productive zone. Usually, the VGPM holds good for Case I waters (where the optical properties are mainly controlled by phytoplankton biomass). However, some studies have shown that modification or parameterization the VGPM can give better results in Case II waters too (Tripathy et al. 2012). From the bio-optical observations it can be classified that the study area is close to the Case I rather than Case II waters. The high CDOM and detrital absorption at some stations (Fig. 5) north of the PF might have been produced locally (autochthonous) due to phytoplankton degradation driven by the heterotrophic microbial activities (Matsuoka et al. 2015). However, the role of freshwater influx originating from melt-ice (Sabu et al. 2014), and winter residue of Antarctic surface water (Tripathy et al. 2015) at the surface and subsurface layer, respectively, could not be ruled out. Both these water masses can contribute towards enhanced a_{CDOM} at PF. Results showed that the overestimation by VGPM was particularly high where the a_{CDOM} values were higher. Furthermore, using weekly satellite Chl-a data (daily data were not available) could have also led to this discrepancy. Nevertheless, from the observed good agreement between in situ and satellite-based IPP it can be inferred that VGPM in its original formulation holds reasonably well even in this area characterized by complex optical properties. Though, Hirawake et al. (2011), Jasmine et al. (2009) also reported good agreement between in situ and satellite-based IPP in this sector; we postulate that site-specific tuning of the embedded VGPM parameters would better reproduce the measured IPP variability in the study area.

Fast repetition rate fluorometry-based observations

Phytoplankton photosynthetic parameters could be derived from the vertical profiling of FRRf. The low F_v/F_m (photochemical efficiency) values in the surface layers can be

linked to deficit of trace nutrients (presumably iron) in this region (Kolber et al. 1988; Boyd and Abraham 2001). Lowest surface F_v/F_m values at PF1 could be due the shallow mixed layer, in which cells were more exposed to a longer daylength (Cheah et al. 2013) or possible time-of-day effect (Aardema et al. 2019; Hughes et al. 2020) that might trigger increased photoinactivation in phytoplankton. The F_v/F_m showed a clear spatial variation but did not show any relation with ambient macronutrient concentrations. The σ_{PSII} (functional absorption cross-section) showed lower values at surface layer and increased with depth to reach maximum at 60 m and thereafter variation of σ_{PSII} as a function of depth remained more or less constant (Fig. 6c, d). Both σ_{PSII} and σ'_{PSII} exhibited a similar vertical distribution pattern with slightly lower values towards surface layers. Unlike F_v/F_m, decrease in surface values was less apparent in case of σ_{PSII}. Both F_v/F_m and σ_{PSII} showed a weak exponential decrease with increasing light intensity (Fig. 6e, f) but showed no relation with ambient macronutrient concentrations. However, no clear relationship between these two parameters was observed. There are reports of inverse relationship between these two photosynthetic parameters from area between Falkland Islands and South of Georgia in SO (Holeton 2005), which was attributed to nutrient limitation. From our present observations, a clear dominance of any phytoplankton size class could not be inferred.

An attempt was made to understand the physiological status of the SO phytoplankton during the current study. The low F_v/F_m and σ_{PSII} values observed in response to high in situ PAR in the surface layers at all stations might be due to the effects of non-photochemical quenching (Hughes et al. 2018, 2020) through which the phytoplankton dissipated some excessive excitation energy and thereby lessened the excitation pressure on PSII (Kolber and Falkowski 1993; Raateoja et al. 2009). The presence of NPQ_{NSV} highlight the probability of saturated electron transport system which might have resulted in low F_v/F_m and σ_{PSII} values observed during the study. The variability in vertical profiles of F_v/F_m and F'_q/F'_m was, however, not reflected in σ_{PSII}. We attribute the absence of clear variability in functional absorption cross-section in spite of variable F_v/F_m and F'_q/F'_m to the presence of NPQ_{NSV} in the dark chamber which lead to a saturated Electron Transport System (ETS) due to higher PAR at surface or inhibitory quenching (Horton et al. 1996). Xu et al. (2018) have reported similar results to those observed by us and attributed the variability of magnitude to conditions like NPQ, phytoplankton taxa present and responses (like photoinactivation) of σ_{PSII} to the light condition.

Vertical mixing exposes the phytoplankton to excessive light at the surface, which results in stressed conditions (Cheah et al. 2013). Earlier reports have shown that the STF is dominated by smaller phytoplankton (Tripathy et al. 2014, 2015) due to macronutrient depleted condition. Nutrient ratios of this study (Table 2) also implied N and Si limitation in this area. In a nutritionally replete environment, phytoplankton cells can attain a maximum F_v/F_m value of 0.65 (Kolber and Falkowski 1993). F_v/F_m value < 0.4 have been an indicative of iron-stressed phytoplankton in the SO (Olson et al. 2000; Boyd and Abraham 2001; Gervais et al. 2002), whereas values higher than 0.5 generally are indicative of little or no nutrient limitation (Behrenfeld et al. 2006). Based on the well-known status of the study region, it likely suggests the probability of the cells being Fe-limited (however, no explicit measurements for Fe could be carried out in our study). From our observations it can be inferred that (i) the phytoplankton were micronutrient (presumably Fe)-starved especially at upper layer and (ii) there was a reduction in the extent of nutrient limitation with depth.

Bio-optical variability and absorption budget

We examined the spectral absorption coefficients of phytoplankton, non-phytoplankton particles and CDOM to understand the bio-optical characteristics of the study area. The carotenoids are known to absorb between 440 to 530 nm with peaks at 460 and 490 nm (Alcantara et al. 2016). The peaks observed between this range were therefore attributed to carotenoids among the a_{ph} spectra measured. The absorption peak at 675 nm was attributed to absorption by Chl-a and Phaeophytin (Alcantara et al. 2016). The a_{ph} (443) and a_{ph} (676) as a function of Chl-a are consistent with studies done at higher latitudes (Wang et al. 2005; Matsuoka et al. 2007; Naik et al. 2010). The variability in relationship between Chl-a and a_{ph} could be due to changes in intracellular concentration of phytoplankton pigments and usually the relationship between a_{ph} and Chl-a varies depending upon nature and concentration of phytoplankton pigments (Bricaud et al. 1998; Ferreira et al. 2013). Furthermore, the contribution of a_{ph} (443) and a_{nph} (443) to a_p (443) is highly variable at lower Chl-a concentrations (< 0.5 mg m^{-3}). The observed inverse relationship between the ratio of a_{nph} to a_p at 443 nm with Chl-a (Fig. 9d) implied an increase in a_{nph} (443) relative to a_{ph} (443) (Bricaud et al. 2010; Kheireddine et al. 2018) as reported from Pacific Ocean indicating presence of large amount of non-phytoplankton particles or CDOM. Thus, it can be inferred that varying contributions of non-phytoplankton particles (i.e. viruses, bacteria, detritus and inorganic particles) have an important role in light absorption in the study area. The relation between phytoplankton absorption coefficient and PP ($R^2 = 0.36$) yielded a stronger relationship than Chl-a and PP ($R^2 = 0.32$) corroborating the hypothesis that variability in PP can be better explained by phytoplankton light absorption than Chl-a (Marra et al. 2007). The a_{ph} (443) and a_p (676) as a function

of Chl-a are weaker in the study area, which implies a lower contribution of a_{ph} to the total absorption. The results are comparable with studies carried out at higher latitude (Wang et al. 2005; Naik et al. 2010).

The $a^*_{ph}(\lambda)$ signifies light absorption efficiency of phytoplankton for photosynthesis and is a key factor to estimate PP (Platt and Sathyendranath 1988; Robinson et al. 2017). Higher mean values of a_{ph} and a^*_{ph} at surface than the DCM indicates higher phytoplankton absorption and Chl-a specific absorption at surface (Fig. 7a–d); further more variability in a_{ph} and a^*_{ph} was noticed at surface than at DCM. The a^*_{ph} were much higher than the a_{ph}, which could be ascribed to adaptation of dominant phytoplankton group (presumed to be smaller size) to the ambient light condition, resulting in better light harvest (Matsuoka et al. 2009). High a^*_{ph} values in the surface and DCM layer of STF could be attributed to the prevalence of smaller phytoplankton as observed by nutrient ratios and PAR–P^B relationship (absence of photoinhibition). Tripathy et al. (2014) reported very high values of P^B at STF due to predominance of smaller phytoplankton. The inverse relationship between a^*_{ph} (443, 676) and nutrient concentration (data not shown) could be due to the high a_{ph} value observed at N-limited STF. The positive correlation between a_{ph} (443) and temperature ($R^2 = 0.58$), and that between a_{ph} (676) and temperature ($R^2 = 0.59$) suggest higher absorption in comparatively warmer stations like SAF and STF. Kheireddine et al. (2018) have reported high a^*_{ph} (443) values at warmer and high saline waters in Red Sea, which was usually dominated by picoplankton.

The ternary diagram (Fig. 8) showing contribution of optically active constituents (a_{CDOM}, a_{nph} and a_{ph}) to the total absorption budget indicates a clear dominance of a_{CDOM} at all stations except at PF2b where the a_{nph} had maximum contribution (61.23%). The a_{ph} contributed nearly 10% to the total absorption budget indicating that absorption in surface waters are under the strong influence of materials other than phytoplankton. The negative relationship between TSM and temperature (figure not shown) indicates the intrusion of cooler waters from south (coastal Antarctica) bringing in more TSM to these areas. Towards the north, the TSM concentrations decreased as also evidenced from the a_{nph} values from the ternary plot. From the positive relationship between a_{CDOM} and water temperature it can be inferred that formation of CDOM is predominant in warmer waters or is being transported by warmer waters from surrounding areas. The ternary plot shows that the CDOM contribution was higher at STF and SAF, even though higher values were also noticed at PF1a and PF2a; it could possibly be due to the allochthonous (originated from outside of that area) materials brought by the meltwater from coastal Antarctica. Sabu et al. (2014) have shown that anomalous phytoplankton bloom reported in this area was triggered by the nutrient-laden freshwater influx originating from ice-melt in coastal Antarctica. The weak positive correlation between Chl-a and a_{CDOM} (440), a_{CDOM} (412) also indicated presences of sources other than phytoplankton (Fig. 9e, f). Balch et al. (2014) have reported similar findings from Arctic waters. The inverse relationship of TSM with Chl-a (Fig. 9g) indicated higher concentration of TSM at surface layer than DCM where phytoplankton biomass was higher, whereas its positive relationship with a_{CDOM} (Fig. 9h) implied their co-variability or probable origin from similar sources supporting the above observation.

Pigment packaging effect

Increase in Chl-a concentration is usually associated with an increase in intracellular pigment concentration or cell volume, which leads to decrease in phytoplankton light absorption efficiency (i.e. lack in correlation between light-harvesting efficiency and pigment packaging originating from intracellular overlap of the chloroplasts on one another) popularly known as "package effect" (Bricaud et al. 1995). It has been proved that increase in pigment concentration or cell volume also results in decrease in P^B or assimilation number (Marra et al. 2007). The observed photoinhibition in the surface layer of PF2 could be ascribed to package effect or the higher daily PAR (Fig. 4d) at PF2 could have caused the observed photoinhibition irrespective of plankton size class. Usually large (> 10 µm) phytoplankton are prone to strong packaging effect, resulting in low Chl-a specific absorption, and vice versa (Bricaud et al. 1995). Previously, Tripathy et al. (2014) have reported photoinhibition in coastal Antarctic stations (65° S) and no photoinhibition at north of 50° S and attributed the photoinhibition to pigment packaging in larger phytoplankton predominant in coastal waters.

To evaluate pigment packaging, we also used Q^*_a (676), the indicator of pigment packaging effect, because light absorption is not influenced by accessory pigments at 676 nm (Matsuoka et al. 2009). The Q^*_a value theoretically varies between 0 (maximum package effect) and 1 (no package effect) (Alcantara et al. 2016). The moderate inverse relationship between Q^*_a (676) and Chl-a, and the values (< 1) for Q^*_a (676) implied packaging effect at PF2b (Fig. 10c). Q^*_a values for other stations indicated no package effect. This is in accordance with the observed PAR–P^B relationship, which shows no photoinhibition at surface layer at STF, SAF and PF1a and could be attributed to the presence of smaller phytoplankton as supported by nutrient data. However, Q^*_a (676) ratios at SAF and PF2b at DCM indicated package effect. It has been shown that DCM in SO is usually dominated by larger phytoplankton (Gomi et al. 2010; Tripathy et al. 2015), which are prone to pigment packaging. From our observations it can inferred that the surface and DCM waters are dominated by smaller and larger phytoplankton, respectively. Q^*_a (676) values higher

than the theoretical maximum could be due to the "associated uncertainties" in path-length amplification β factor (i.e. the ratio of optical to geometrical path-length) in laboratory measurements, which increases with decreasing optical density (Bricaud and Stramski 1990; Alcantara et al. 2016).

Most of the a^*_{ph} (λ) values in our study, were > 0.05 m^2 mgChl-a^{-1} are an indicative of less packaging effect or higher concentrations of non-photosynthetic pigments, implying the presence of smaller phytoplankton (Bricaud et al. 2010) at the sampling locations. Considerable light absorption by accessory pigments, is known to have an impact on a^*_{ph} estimates that vary across the blue to red spectral range. The packaging effect observed at nutrient replete PF2 region could be corroborated by the large variability observed in a^*_{ph} in the blue spectrum (at 443 nm) than the red spectrum (at 676 nm) or changes in pigment composition (Bricaud et al. 1998). Though our dataset does not allow us explain the process involved; studies (Palmisano et al. 1986; Mendes et al. 2015) have shown that phytoplankton can modulate their photosynthetic efficiency when subjected to changing light intensity in the Polar Regions. Pigment packaging has been observed to be significant at high latitude marine ecosystems as phytoplankton acclimate themselves to the low-light and high-nutrient environment (Cota et al. 2003).

Deriving phytoplankton size classes from in situ radiometric measurements

Variation in phytoplankton absorption characteristics were used to classify the surface phytoplankton community structure in the study area. The blue to red ratio (*B*/*R*) from spectrophotometric and radiometric measurements of a_{ph} indicated the dominance of small phytoplankton in the surface waters in all stations except at PF2b, where the spectrophotometric *B*/*R* was 1.09 implying microplankton dominance. In principle, if the *B*/*R* is > 3.0, it indicates dominance of picophytoplankton (< 2 µm). If the ratio is < 2.5, dominance of microphytoplankton (> 20 µm) is implied (Hirata et al. 2008). Ratios between 2.5 and 3.0 indicate nanophytoplankton predominance in the phytoplankton community structure (Aguilar-Maldonado et al. 2018). From the observed nutrient ratios in the study area it is inferred that the environment was not conducive (N and Si-limited) for large phytoplankton, which could have led to succession by smaller ones in the surface waters. The blue to red ratio of a^*_{ph} is used as proxy of phytoplankton size, where higher values (> 3) of a^*_{ph} (443)/a^*_{ph} (676) are associated with smaller cells (Lohrenz et al. 2003). All the stations in the study area, exhibited predominance of relatively smaller size phytoplankton and hence less or no package effect as reported elsewhere by Naik et al. (2013), which corroborates our observations discussed in previous sections. The moderate relationship of radiometer-derived K_d (490) with in situ Chl-a and a_{ph} (490) (Fig. 11c, d) indicates that the factors other than phytoplankton biomass (such as a_{nph}, a_{CDOM} and TSM) also influence the light attenuation in the water column. The comparative result for modelled K_d (490) and the averaged depth value of in situ K_d for downwelling irradiance indicated that the modelled K_d (490) calculated using the upper 20 m depth could explain most of the variability (71%) in the in situ K_d (490) indicating maximum optical variability in the upper layers (~ 120 m). In situ R_{rs}-based Chl-a was retrieved using OC2, OC3 and OC4 (version 6) algorithms designed for SeaWiFS, which showed a good correlation with measured Chl-a and explained ~ 75% of variability in it (Fig. 11f), implying that global algorithms hold reasonably well in this region.

Summary and conclusions

The current study highlights variability in phytoplankton productivity and bio-optical characteristics in the lesser explored Indian sector of the Southern Ocean. The in situ productivity estimation indicates STF to be the most productive region, whereas PF2b as the least, which is well supported by the FRRf-based photosynthetic measurements. The subsurface PP maxima can be regarded as an indicator of photoinhibition/micronutrient limitation in the surface layers. High integrated PP at STF was associated with high concentrations of Chl-a and a shallow DCM. The observed agreement between in situ and satellite-based Chl-a and PP revealed that global models in their original formulation would function well in the study area in spite of its complex optical properties. Nitrogen limitation at the STF was associated with presence of small sized phytoplankton with better light-harvesting capacity, which was corroborated by bio-optical measurements. A low to moderate (0.1–0.4) F_v/F_m indicated overall reduced phytoplankton photosynthetic efficiency in the study area. The in situ absorption measurements and ratios between remote sensing reflectance-derived phytoplankton absorption at blue/red band indicated dominance of smaller phytoplankton (less or no pigment packaging effect) in the surface, whereas larger phytoplankton (prone to pigment packaging) at the DCM. Low contribution of a_{ph} to the total absorption budget implied that surface waters were under a strong influence of non-phytoplankton materials.

It can hence be inferred that changes in ambient physical environment in terms of light and nutrient availability, and bio-optical characteristics could modulate phytoplankton size class and thereby productivity more critically in surface than in the deeper layers of ISSO. The current study fairly improves our understanding of PP estimates and bio-optical variability in this sparsely sampled region. We recommend

a long-term monitoring of PP and bio-optical variables with emphasis on surrounding physicochemical environment to know the changing mechanisms of carbon-sequestration better. Such concerted efforts will improve the current understanding about the contribution of SO in the global carbon cycle and its potential role in climate change scenario.

Acknowledgements The authors thank Ministry of Earth Sciences, Government of India for financial support. Our thanks are also due to the Director, National Centre for Polar and Ocean Research (NCPOR) for constant encouragement. We thank the captain, officers and all the crew members of ORV-*Sagar Nidhi* for their invaluable help during the expedition. We are grateful to Dr. David Hughes for his valuable suggestions about interpretation of the FRRf data, Dr. Jill Schwarz and the anonymous reviewer for their insightful suggestions that led to an overall improvement of the manuscript. Ms. Anvita Ulhas Kerkar is grateful to the Department of Science and Technology, Government of India for DST-INSPIRE doctoral research fellowship and Goa University, Goa for research administrative facilities. This is NCPOR Contribution Number J-43/2020-21.

Conflict of interest We declare that the authors do not have any conflict of interest.

References

Aguilar-Maldonado J, Santamaría-del-Ángel E, González-Silvera A, Cervantes-Rosas O, López L, Gutiérrez-Magness A, Cerdeira-Estrada S, Sebastiá-Frasquet MT (2018) Identification of phytoplankton blooms under the index of Inherent Optical Properties (IOP index) in optically complex waters. Water 10(2):129. https://doi.org/10.3390/w10020129

Alcântara E, Watanabe F, Rodrigues T, Bernardo N (2016) An investigation into the phytoplankton package effect on the chlorophyll-a specific absorption coefficient in Barra Bonita reservoir, Brazil. Remote Sens Lett 8:761–770. https://doi.org/10.1080/2150704X.2016.1185189

Amante C, Eakins BW (2009) ETOPO1 1 arc-minute global relief model: procedures, data sources and analysis. NOAA Technical Memorandum NESDIS NGDC-24. National Geophysical Data Center NOAA, Boulder

Aardema HM, Rijkeboer M, Lefebvre A, Veen A, Kromkamp JC (2019) High-resolution underway measurements of phytoplankton photosynthesis and abundance as an innovative addition to water quality monitoring programs. Ocean Sci 15(5):1267–1285. https://doi.org/10.5194/os-15-1267-2019

Arrigo KR, van Dijken G, Long M (2008) A strong anthropogenic CO_2 sink. Geophys Res Lett. https://doi.org/10.1029/2008GL035624

Babin M, Stramski D, Ferrari GM, Claustre H, Bricaud A, Obolensky G, Hoepffner N (2003) Variations in the light absorption coefficients of phytoplankton, nonalgal particles, and dissolved organic matter in coastal waters around Europe. J Geophys Res. https://doi.org/10.1029/2001JC000882

Balch WM, Bowler BC, Lubelczyk LC, Stevens MW Jr (2014) Aerial extent, composition, bio-optics and biogeochemistry of a massive under-ice algal bloom in the Arctic. Deep Res Part II 105:42–58. https://doi.org/10.1016/j.dsr2.2014.04.001

Behrenfeld MJ, Falkowski PG (1997a) Photosynthetic rates derived from satellite-based chlorophyll concentration. Limnol Oceanogr 1:1–20

Behrenfeld MJ, O'Malley RT, Siegel DA, McClain CR, Sarmiento JL, Feldman GC, Milligan AJ, Falkowski PG, Letelier RM, Boss ES (2006) Climate-driven trends in contemporary ocean productivity. Nature 444(7120):752. https://doi.org/10.1038/nature05317

Behrenfeld MJ, Falkowski PG (1997b) A consumer's guide to phytoplankton primary productivity models. Limnol Oceanogr 42(7):1479–1491

Belkin IM, Gordon AL (1996) Southern Ocean fronts from the Greenwich meridian to Tasmania. J Geophys Res: Oceans 101(C2):3675–3696

Blain S, Trehguer P, Belviso S, Bucciarelli E, Denis M, Desabre S, Fiala M, Jehzehque VM, Fevre JL, MayzaudP, Marty JC, Razouls S (2001) A biogeochemical study of the island mass effect in the context of the ironhypothesis: Kerguelen Islands, Southern Ocean. Deep Sea Res I 48:163–187. https://doi.org/10.1016/S0967-0637(00)00047-9

Boyd PW (2002) Environmental factors controlling phytoplankton processes in the Southern Ocean1. J Phycol 38(5):844–861. https://doi.org/10.1046/j.1529-8817.2002.t01-1-01203.x

Boyd PW, Abraham ER (2001) Iron-mediated changes in phytoplankton photosynthetic competence during SOIREE. Deep Res Part II 48(11–12):2529–2550. https://doi.org/10.1016/S0967-0645(01)00007-8

Bricaud A, Babin M, Morel A, Claustre H (1995) Variability in the chlorophyll-specific absorption coefficients of natural phytoplankton: analysis and parameterization. J Geophys Res: Oceans 100(C7):13321–13332

Bricaud A, Morel A, Babin M, Allali K, Claustre H (1998) Variations of light absorption by suspended particles with chlorophyll a concentration in oceanic (case 1) waters: analysis and implications for bio-optical models. J Geophys Res 103(C13):31033–31044

Bricaud A, Babin M, Claustre H, Ras J, Tièche F (2010) Light absorption properties and absorption budget of Southeast Pacific waters. J Geophys Res. https://doi.org/10.1029/2009JC005517

Bricaud A, Claustre H, Ras J, Oubelkheir K (2004) Natural variability of phytoplanktonic absorption in oceanic waters: Influence of the size structure of algal populations. J Geophys Res. https://doi.org/10.1029/2004JC002419

Bricaud A, Stramski D (1990) Spectral absorption coefficients of living phytoplankton and nonalgal biogenous matter: a comparison between the Peru upwelling area and the Sargasso Sea. Limnol Oceanogr 35(3):562–582

Cheah W, McMinn A, Griffiths FB, Westwood KJ, Wright SW, Clementson LA (2013) Response of phytoplankton photophysiology to varying environmental conditions in the Sub-antarctic and polar frontal zone. PLoS ONE 8(8):e72165. https://doi.org/10.1371/journal.pone.0072165

Cleveland JS, Weidemann AD (1993) Quantifying absorption by aquatic particles: a multiple scattering correction for glass-fiber filters. Limnol Oceanogr 38(6):1321–1327

Cota GF, Harrison WG, Platt T, Sathyendranath S, Stuart V (2003) Bio-optical properties of the Labrador Sea. J Geophys Res. https://doi.org/10.1029/2000jc000597

Cullen JJ (1982) The deep chlorophyll maximum: comparing vertical profiles of chlorophyll a. Can J Fish Aquat Sci 39(5):791–803

Ferreira A, Stramski D, Garcia CA, Garcia VM, Ciotti ÁM, Mendes CR (2013) Variability in light absorption and scattering of phytoplankton in Patagonian waters: role of community size structure and pigment composition. J Geophys Res 118(2):698–714. https://doi.org/10.1002/jgrc.20082

Froneman PW, Pakhomov EA, Perissinotto R, Laubscher RK, McQuaid CD (1997) Dynamics of the plankton communities of the Lazarev Sea (Southern Ocean) during seasonal ice melt. Mar Ecol Prog Ser 149:201–214

Gandhi N, Ramesh R, Laskar AH, Sheshshayee MS, Shetye S, Anilkumar N, Patil SM, Mohan R (2012) Zonal variability in primary production and nitrogen uptake rates in the southwestern

Indian Ocean and the Southern Ocean. Deep-Sea Res Part I 67:32–43. https://doi.org/10.1016/j.dsr.2012.05.003
Gervais F, Riebesell U, Gorbunov MY (2002) Changes in primary productivity and chlorophyll a in response to iron fertilization in the Southern Polar Frontal Zone. Limnol Oceanogr 47(5):1324–1335. https://doi.org/10.4319/lo.2002.47.5.1324
Gomi Y, Fukuchi M, Taniguchi A (2010) Diatom assemblages at subsurface chlorophyll maximum layer in the eastern Indian sector of the Southern Ocean in summer. J Plankton Res 32(7):1039–1050. https://doi.org/10.1093/plankt/fbq031
Graham RM (2014) The role of Southern Ocean fronts in the global climate system (Doctoral dissertation, Department of Geological Sciences, Stockholm University)
Hirata T, Aiken J, Hardman-Mountford N, Smyth TJ, Barlow RG (2008) An absorption model to determine phytoplankton size classes from satellite ocean colour. Remote Sens Environ 112(6):3153–3159. https://doi.org/10.1016/j.rse.2008.03.011
Hirawake T, Takao S, Horimoto N, Ishimaru T, Yamaguchi Y, Fukuchi M (2011) A phytoplankton absorption-based primary productivity model for remote sensing in the Southern Ocean. Polar Biol 34:291–302. https://doi.org/10.1007/s00300-010-0949-y
Holeton CL, Nedelec F, Sanders R, Brown L, Moore CM, Stevens DP, Heywood KJ, Statham PJ, Lucas CH (2005) Physiological state of phytoplankton communities in the Southwest Atlantic sector of the Southern Ocean, as measured by fast repetition rate fluorometry. Polar Biol 29:44–52. https://doi.org/10.1007/s00300-005-0028-y
Holliday NP, Read JF (1998) Surface oceanic fronts between Africa and Antarctica. Deep Sea Res I Part I 45(2–3):217–238
Horton P, Ruban AV, Walters RG (1996) Regulation of light harvesting in green plants. Annu Rev Plant Physiol Plant Mol Biol 47:655–684. https://doi.org/10.1146/annurev.arplant.47.1.655
Hughes DJ, Campbell DA, Doblin MA, Kromkamp JC, Lawrenz E, Moore CM, Suggett DJ (2018) Roadmaps and detours: active chlorophyll-a assessments of primary productivity across marine and freshwater systems. Environ Sci Technol 52(21):12039–12054. https://doi.org/10.1021/acs.est.8b03488
Hughes DJ, Croswell JR, Doblin MA, Oxborough K, Ralph PJ, Varkey D, Suggett DJ (2020) Dynamic variability of the phytoplankton electron requirement for carbon fixation in eastern Australian waters. J Marine Syst 202:103252. https://doi.org/10.1016/j.jmarsys.2019.103252
Jasmine P, Muraleedharan KR, Madhu NV, Devi CA, Alagarsamy R, Achuthankutty CT, Jayan Z, Sanjeevan VN, Sahayak S (2009) Hydrographic and productivity characteristics along 45 E longitude in the southwestern Indian Ocean and Southern Ocean during Austral summer 2004. Mar Ecol Prog Ser 389:97–116
Kemp AE, Grigorov I, Pearce RB, Garabato AN (2010) Migration of the Antarctic Polar Front through the mid-Pleistocene transition: evidence and climatic implications. Quaternary Sci Rev 29(17–18):1993–2009. https://doi.org/10.1016/j.quascirev.2010.04.027
Kheireddine M, Ouhssain M, Organelli E, Bricaud A, Jones BH (2018) Light absorption by suspended particles in the Red Sea: effect of phytoplankton community size structure and pigment composition. J Geophys Res: Oceans 123(2):902–921. https://doi.org/10.1002/2017JC013279
Kirk JT (1994) Light and photosynthesis in aquatic ecosystems. Cambridge University Press, Cambridge
Kishino M, Takahashi M, Okami N, Ichimura S (1985) Estimation of the spectral absorption coefficients of phytoplankton in the sea. Bull Mar Sci 37(2):634–642
Knap AH, Michaels A, Close AR, Ducklow H, Dickson AG. (1996) Protocols for the joint global ocean flux study (JGOFS) core measurements.
Kolber Z, Falkowski PG (1993) Use of active fluorescence to estimate phytoplankton photosynthesis in situ. Limnol Oceanogr 38(8):1646–1665
Kolber Z, Zehr J, Falkowski P (1988) Effects of growth irradiance and nitrogen limitation on photosynthetic energy conversion in photosystem II. Plant Physiol 88(3):923–929
Kostianoy AG, Ginzburg AI, Frankignoulle M, Delille B (2004) Fronts in the Southern Indian Ocean as inferred from satellite sea surface temperature data. J Mar Syst 45(1–2):55–73. https://doi.org/10.1016/j.jmarsys.2003.09.004
Le Quéré C, Rödenbeck C, Buitenhuis ET, Conway TJ, Langenfelds R, Gomez A, Labuschagne C, Ramonet M, Nakazawa T, Metzl N, Gillett N (2007) Saturation of the Southern Ocean CO_2 sink due to recent climate change. Science 316(5832):1735–1738. https://doi.org/10.1126/science.1136188
Lee ZP, Carder KL, Arnone RA (2002) Deriving inherent optical properties from water color: a multiband quasi-analytical algorithm for optically deep waters. Appl Opt 41:5755–5772. https://doi.org/10.1364/AO.41.005755
Lee ZP, Weidemann A, Kindle J, Arnone R, Carder KL, Davis C (2007) Euphotic zone depth: Its derivation and implication to ocean-color remote sensing. J Geophys Res. https://doi.org/10.1126/science.1136188
Levasseur ME, Therriault JC (1987) Phytoplankton biomass and nutrient dynamics in a tidally induced upwelling: the role of the NO_3:SiO_4 ratio. Mar Ecol Prog Ser 39:87–97
Lohrenz SE, Weidemann AD, Tuel M (2003) Phytoplankton spectral absorption as influenced by community size structure and pigment composition. J Plankton Res 25(1):35–61. https://doi.org/10.1093/plankt/25.1.35
Marra J, Trees CC, O'Reilly JE (2007) Phytoplankton pigment absorption: a strong predictor of primary productivity in the surface ocean. Deep-Sea Res Part I 54(2):155–163. https://doi.org/10.1016/j.dsr.2006.12.001
Matsuoka A, Huot Y, Shimada K, Saitoh SI, Babin M (2007) Bio-optical characteristics of the western Arctic Ocean: implications for ocean color algorithms. Can J Remote Sens 33(6):503–518
Matsuoka A, Larouche P, Poulin M, Vincent W, Hattori H (2009) Phytoplankton community adaptation to changing light levels in the southern Beaufort Sea. Can Arctic Estuar Coast Mar Sci 82(3):537–546. https://doi.org/10.1016/j.ecss.2009.02.024
Matsuoka A, Ortega-Retuerta E, Bricaud A, Arrigo KR, Babin M (2015) Characteristics of colored dissolved organic matter (CDOM) in the Western Arctic Ocean: relationships with microbial activities. Deep Res Part II 118:44–52. https://doi.org/10.1016/j.dsr2.2015.02.012
Mendes CR, Tavano VM, Dotto TS, Kerr R, De Souza MS, Garcia CA, Secchi ER (2018) New insights on the dominance of cryptophytes in Antarctic coastal waters: a case study in Gerlache Strait. Deep Res Part II 149:161–170. https://doi.org/10.1016/j.dsr2.2017.02.010
Mendes CR, Kerr R, Tavano VM, Cavalheiro FA, Garcia CA, Dessai DR, Anilkumar N (2015) Cross-front phytoplankton pigments and chemotaxonomic groups in the Indian sector of the Southern Ocean. Deep Res Part II 118:221–232. https://doi.org/10.1016/j.dsr2.2015.01.003
Mengesha S, Dehairs F, Fiala M, Elskens M, Goeyens L (1998) Seasonal variation of phytoplankton community structure and nitrogen uptake regime in the Indian Sector of the Southern Ocean. Polar Biol 20(4):259–272. https://doi.org/10.1007/s003000053002
Mitchell BG (1990) Algorithms for determining the absorption coefficient for aquatic particulates using the quantitative filter technique. In: Spinrad RW (ed) Ocean optics X Sep 1. International Society for Optics and Photonics, Bellingham
Mitchell BG, Kahru M, Wieland J, Stramska M, Mueller JL (2002) Determination of spectral absorption coefficients of particles,

dissolved material and phytoplankton for discrete water samples. Ocean Opt Protoc Satellite Ocean Color Sensor Valid 3(2):231

Moline MA, Claustre H, Frazer TK, Schofield O, Vernet M (2004) Alteration of the food web along the Antarctic Peninsula in response to a regional warming trend. Glob Change Biol 10(12):1973–1980. https://doi.org/10.1111/j.1365-2486.2004.00825.x

Moore CM, Suggett D, Holligan PM, Sharples J, Abraham ER, Lucas MI, Rippeth TP, Fisher NR, Simpson JH, Hydes DJ (2003) Physical controls on phytoplankton physiology and production at a shelf sea front: a fast repetition-rate fluorometer based field study. Mar Ecol Prog Ser 259:29–45. https://doi.org/10.3354/meps259029

Moore JK, Abbott MR, Richman JG (1999) Location and dynamics of the Antarctic Polar Front from satellite sea surface temperature data. J Geophys Res 104(C2):3059–3073

Morel A, Berthon JF (1989) Surface pigments, algal biomass profiles, and potential production of the euphotic layer: relationships reinvestigated in view of remote-sensing applications. Limnol Oceanogr 34(8):1545–1562

Naik P, D'Sa E, Goesdo Rosario Gomes JIH (2010) Assessment of particulate absorption properties in the southeastern Bering Sea from in-situ and remote sensing data. J Appl Remote Sens 4(1):043561. https://doi.org/10.1117/1.3525572

Naik P, D'Sa EJ, Gomes HD, Goés JI, Mouw CB (2013) Light absorption properties of southeastern Bering Sea waters: analysis, parameterization and implications for remote sensing. Rem Sens Environ 134:120–134. https://doi.org/10.1016/j.rse.2013.03.004

Olbers D, Borowski DA, Völker C (2004) The dynamical balance, transport and circulation of the Antarctic Circumpolar Current. Antarct Sci 16(4):439–470. https://doi.org/10.1017/S0954102004002251

Olson RJ, Sosik HM, Chekalyuk AM, Shalapyonok A (2000) Effects of iron enrichment on phytoplankton in the Southern Ocean during late summer: active fluorescence and flow cytometric analyses. Deep Res Part II 47(15–16):3181–3200. https://doi.org/10.1016/S0967-0645(00)00064-3

Orsi AH, Whitworth T III, Nowlin WD Jr (1995) On the meridional extent and fronts of the Antarctic Circumpolar Current. Deep-Sea Res Part I 42(5):641–673

Oxborough K, Moore CM, Suggett DJ, Lawson T, Chan HG, Geider RJ (2012) Direct estimation of functional PSII reaction center concentration and PSII electron flux on a volume basis: a new approach to the analysis of Fast Repetition Rate fluorometry (FRRf) data. Limnol Oceanogr 10(3):142–154. https://doi.org/10.4319/lom.2012.10.142

Palmisano AC, SooHoo JB, SooHoo SL, Kottmeier ST, Craft LL, Sullivan CW (1986) Photoadaptation in *Phaeocystispouchetii* advected beneath annual sea ice in McMurdo Sound, Antartica. J Plankton Res 8(5):891–906

Parslow JS, Boyd PW, Rintoul SR, Griffiths FB (2001) A persistent subsurface chlorophyll maximum in the Interpolar Frontal Zone south of Australia: seasonal progression and implications for phytoplankton- light-nutrient interactions. J Geophys Res 106:31543–31557. https://doi.org/10.1029/2000JC000322

Pavithran S, Anilkumar N, Krishnan KP, Noronha SB, George JV, Nanajkar M, Chacko R, Dessai DR, Achuthankutty CT (2012) Contrasting pattern in chlorophyll a distribution within the Polar Front of the Indian sector of Southern Ocean during austral summer 2010. Curr Sci 102(6):899

Platt T, Sathyendranath S (1988) Oceanic primary production: estimation by remote sensing at local and regional scales. Science 241(4873):1613–1620

Pond S, Pickard GL (1978) Introductory dynamical oceanography. Pergamon Press, New York

Pope RM, Fry ES (1997) Absorption spectrum (380–700 nm) of pure water. II. Integrating cavity measurements. Appl Opt 36(33):8710–8723

Prakash S, Ramesh R, Sheshshayee MS, Mohan R, Sudhakar M (2015) Nitrogen uptake rates and f-ratios in the Equatorial and Southern Indian Ocean. Curr Sci 108:239–245

Raateoja M, Mitchell BG, Wang H, Olivo E (2009) Effect of water column light gradient on phytoplankton fluorescence transients. Mar Ecol Prog Ser 376:85–101. https://doi.org/10.3354/meps07759

Redfield AC (1963) The influence of organisms on the composition of seawater. The sea 2:26–77

Rintoul SR, Sokolov S, Williams MJ, Peña Molino B, Rosenberg M, Bindoff NL (2014) Antarctic circumpolar current transport and barotropic transition at Macquarie Ridge. Geophys Res Lett 41(20):7254–7261. https://doi.org/10.1002/2014GL061880

Rintoul SR, Trull TW (2001) Seasonal evolution of the mixed layer in the Subantarctic Zone south of Australia. J Geophys Res 106(C12):31447–31462. https://doi.org/10.1002/2014GL061880

Robinson CM, Cherukuru N, Hardman-Mountford NJ, Everett JD, McLaughlin MJ, Davies KP, Van Dongen-Vogels V, Ralph PJ, Doblin MA (2017) Phytoplankton absorption predicts patterns in primary productivity in Australian coastal shelf waters. Estuar Coast Shelf Sci 192:1–6. https://doi.org/10.1016/j.ecss.2017.04.012

Sabu P, Anilkumar N, George JV, Chacko R, Tripathy SC, Achuthankutty CT (2014) The influence of air-sea-ice interactions on an anomalous phytoplankton bloom in the Indian Ocean sector of the Antarctic zone of the Southern Ocean during the austral summer. Polar Sci 8:370–384. https://doi.org/10.1016/j.polar.2014.08.001

Sakshaug E, Bricaud A, Dandonneau Y, Falkowski PG, Kiefer DA, Legendre L, Morel A, Parslow J, Takahashi M (1997) Parameters of photosynthesis: definitions, theory and interpretation of results. J Plankton Res. https://doi.org/10.1093/plankt/19.11.1637

Sarmiento JL, Hughes TM, Stouffer RJ, Manabe S (1998) Simulated response of the ocean carbon cycle to anthropogenic climate warming. Nature 393(6682):245

Sathyendranath S, Platt T (2007) Spectral effects in bio-optical control on the ocean system. Oceanologia 49:5–39

Smith WO Jr, Dennett MR, Mathot S, Caron DA (2003) The temporal dynamics of the flagellated and colonial stages of Phaeocystis antarctica in the Ross Sea. Deep Res Part II 50(3–4):605–617. https://doi.org/10.1016/S0967-0645(02)00586-6

Sokolov S, Rintoul SR (2002) Structure of Southern Ocean fronts at 140 E. J Mar Syst 37(1–3):151–184. https://doi.org/10.1016/S0924-7963(02)00200-2

Steele JH (1962) Environmental control of photosynthesis in the sea. Limnol Oceanogr 7(2):137–150

Stramski D, Morel A (1990) Optical properties of photosynthetic picoplankton in different physiological states as affected by growth irradiance. Deep Sea Res Part I37(2):245–266. https://doi.org/10.1016/0198-0149(90)90126-G

Strickland JD, Parsons TR (1972) A practical handbook of seawater analysis. Fisheries Research Board of Canada, Ottawa

Thomalla SJ, Waldron HN, Lucas MI, Read JF, Ansorge IJ, Pakhomov E (2011) Phytoplankton distribution and nitrogen dynamics in the southwest Indian subtropical gyre and Southern Ocean waters. Ocean Sci 7(1):113–127. https://doi.org/10.5194/os-7-113-2011

Tripathy SC, Ishizaka J, Siswanto E, Shibata T, Mino Y (2012) Modification of the vertically generalized production model for the turbid waters of Ariake Bay, southwestern Japan. Estuar Coast Shelf Sci 97:66–77. https://doi.org/10.1016/j.ecss.2011.11.025

Tripathy SC, Ishizaka J, Fujiki T, Shibata T, Okamura K, Hosaka T, Saino T (2010) Assessment of carbon- and fluorescence-based primary productivity in Ariake Bay, southwestern Japan.

Estuar Coast Shelf Sci 87:163–173. https://doi.org/10.1016/j.ecss.2010.01.006

Tripathy SC, Pavithran S, Sabu P, Naik RK, Noronha SB, Bhaskar PV, Kumar NA (2014) Is primary productivity in the Indian Ocean sector of Southern Ocean affected by pigment packaging effect? Curr Sci 107(6):00113891

Tripathy SC, Pavithran S, Sabu P, Pillai HU, Dessai DR, Anilkumar N (2015) Deep chlorophyll maximum and primary productivity in Indian Ocean sector of the Southern Ocean: case study in the Subtropical and Polar Front during austral summer 2011. Deep Res Part II 118:240–249. https://doi.org/10.1016/j.dsr2.2015.01.004

Tripathy SC, Patra S, Vardhan KV, Sarkar A, Mishra RK, Anilkumar N (2018) Nitrogen uptake by phytoplankton in surface waters of the Indian sector of Southern Ocean during austral summer. Front Earth Sci 12(1):52–62. https://doi.org/10.1007/s11707-017-0649-9

Tripathy SC, Jena B (2019) Iron-stimulated phytoplankton blooms in the Southern Ocean: a brief review. Rem Sen Earth Syst Sci 2(1):64–77. https://doi.org/10.1007/s41976-019-00012-y

Trull TW, Bray SG, Manganini SJ, Honjo S, Francois R (2001) Moored sediment trap measurements of carbon export in the Subantarctic and Polar Frontal Zones of the Southern Ocean, south of Australia. J Geophys Res: Oceans 106(C12):31489–31509. https://doi.org/10.1029/2000JC000308

UNESCO (1994) Protocols for the joint global ocean flux study (JGOFS) core measurements. IOC Manual and Guides, 29.

Wang D, Liang S, Liu R, Zheng T (2010) Estimation of daily-integrated PAR from sparse satellite observations: Comparison of temporal scaling methods. Int J Remote Sens 31(6):1661–1677. https://doi.org/10.1080/01431160903475407

Wang SQ, Ishizaka J, Yamaguchi H, Tripathy SC, Hayashi M, Xu YJ, Mino Y, Matsuno T, Watanabe Y, Yoo SJ (2014) Influence of the Changjiang River on the light absorption properties of phytoplankton from the East China Sea. Biogeosciences 11(7):1759–1773. https://doi.org/10.5194/bg-11-1759-2014

Wang J, Cota GF, Ruble DA (2005) Absorption and backscattering in the Beaufort and Chukchi Seas. J Geophys Res. https://doi.org/10.1029/2002JC001653

Webb WL, Newton M, Starr D (1974) Carbon dioxide exchange of *Alnus rubra*. Oecologia 17(4):281–291

Westwood KJ, Griffiths FB, Webb JP, Wright SW (2011) Primary production in the Sub-Antarctic and Polar Frontal zones south of Tasmania, Australia; SAZ-Sense survey, 2007. Deep Res Part II 58(21–22):2162–2178. https://doi.org/10.1016/j.dsr2.2011.05.017

Westwood KJ, Griffiths FB, Meiners KM (2006) Williams GD (2010) Primary productivity off the Antarctic coast from 30–80 E; BROKE-West survey. Deep Res Part II 57(9–10):794–814. https://doi.org/10.1016/j.dsr2.2008.08.020

Wu J, Hong H, Shang S, Dai M, Lee Z (2007) Variation of phytoplankton absorption coefficients in the northern South China Sea during spring and autumn. Biogeosciences 4(3):1555–1584. https://doi.org/10.5194/bgd-4-1555-2007

Xu K, Lavaud J, Perkins R, Austen E, Bonnanfant M, Campbell DA (2018) Phytoplankton σPSII and excitation dissipation; implications for estimates of primary productivity. Front Mar Sci 5:281. https://doi.org/10.3389/fmars.2018.00281